Spectroscopic survey of *Kepler* stars – II. FIES/NOT observations of A- and F-type stars

E. Niemczura,[1]★ M. Polińska,[2]★ S. J. Murphy,[3,4] B. Smalley,[5] Z. Kołaczkowski,[1]
J. Jessen-Hansen,[6] K. Uytterhoeven,[7,8] J. M. Lykke,[9] A. Triviño Hage[7,8]
and G. Michalska[1]

[1]*Instytut Astronomiczny, Uniwersytet Wrocławski, Kopernika 11, PL-51-622 Wrocław, Poland*
[2]*Astronomical Observatory Institute, Faculty of Physics, A. Mickiewicz University, Słoneczna 36, PL-60-286 Poznań, Poland*
[3]*Sydney Institute for Astronomy (SIfA), School of Physics, University of Sydney, NSW 2006, Australia*
[4]*Stellar Astrophysics Centre, Department of Physics and Astronomy, Aarhus University, DK-8000 Aarhus C, Denmark*
[5]*Astrophysics Group, Keele University, Staffordshire ST5 5BG, UK*
[6]*Stellar Astrophysics Centre, Department of Physics and Astronomy, Aarhus University, Ny Munkegade 120, DK-8000 Aarhus C, Denmark*
[7]*Instituto de Astrofisica de Canarias, E-38205 La Laguna, Tenerife, Spain*
[8]*Departamento de Astrofisica, Universidad de La Laguna, E-38206 La Laguna, Tenerife, Spain*
[9]*Centre for Star and Planet Formation, Niels Bohr Institute and Natural History Museum of Denmark, University of Copenhagen,*
Øster Voldgade 5-7, DK-1350 Copenhagen K, Denmark

ABSTRACT

We have analysed high-resolution spectra of 28 A and 22 F stars in the *Kepler* field, observed using the Fibre-Fed Échelle Spectrograph at the Nordic Optical Telescope. We provide spectral types, atmospheric parameters and chemical abundances for 50 stars. Balmer, Fe I and Fe II lines were used to derive effective temperatures, surface gravities and microturbulent velocities. We determined chemical abundances and projected rotational velocities using a spectrum synthesis technique. Effective temperatures calculated by spectral energy distribution fitting are in good agreement with those determined from the spectral line analysis. The stars analysed include chemically peculiar stars of the Am and λ Boo types, as well as stars with approximately solar chemical abundances. The wide distribution of projected rotational velocity, $v\sin i$, is typical for A and F stars. The microturbulence velocities obtained are typical for stars in the observed temperature and surface gravity ranges. Moreover, we affirm the results of Niemczura et al. that Am stars do not have systematically higher microturbulent velocities than normal stars of the same temperature.

Key words: stars: abundances – stars: chemically peculiar – stars: general – stars: rotation.

1 INTRODUCTION

The high-precision *Kepler* photometric time series are excellent for studying the variability of stars across the Hertzsprung–Russell (H–R) diagram (Kjeldsen et al. 2010; Gilliland et al. 2015). The ultrahigh precision and long duration offer unparalleled opportunities to discover and characterize stellar pulsations and consequently to make progress in modelling stellar evolution and internal structure using asteroseismology.

To perform an asteroseismic study, the precise pulsation frequencies, mode identification and atmospheric parameters (effective temperature $T_{\rm eff}$, surface gravity $\log g$, chemical abundances and rotational velocity $v\sin i$) are the necessary factors. Pulsation

frequencies can be determined from the analysis of the precise *Kepler* photometry. The best way to obtain information about atmospheric parameters is the investigation of high-resolution spectra. For this reason, ground-based spectroscopic observations of stars in the *Kepler* field began before the mission (Uytterhoeven et al. 2010).

High- and medium-resolution spectra have been collected and analysed for a substantial number of A- and F-type stars (e.g. Catanzaro et al. 2011; Tkachenko et al. 2012, 2013a,b; Niemczura et al. 2015, hereafter Paper I). The atmospheric parameters obtained in those investigations are of great importance for seismic modelling of δ Scuti, γ Doradus and γ Dor/δ Sct hybrid stars, which occupy this region of the H–R diagram. The hybrid variables are of particular interest, showing g mode as well as p mode pulsations. In such cases, two regions of the stellar interior can be probed because the g modes propagate in the layers between the convective core and the

★ E-mail: niemczura@astro.uni.wroc.pl (EN); polinska@amu.edu.pl (MP)

envelope while the p modes probe the outer layers of the envelope (Guzik et al. 2015).

An additional benefit of studying atmospheric parameters of pulsating A and F stars is the possibility to observationally define instability regions of δ Scuti, γ Doradus and γ Dor/δ Sct hybrids on the H–R diagram. The question of purity of the pulsational instability strips has been addressed with high-resolution spectroscopy once before, when the improvement over Sloan Digital Sky Survey (SDSS) photometry showed the DAV instability strip to be pure (Murphy et al. 2015).

From the analysis of *Kepler* data, Grigahcène et al. (2010) and Uytterhoeven et al. (2011) discovered a large number of hybrid star candidates occupying a region of the T_{eff}–log g diagram broader than predicted by the current stellar pulsation theory (e.g. Guzik et al. 2015). However, the correct interpretation of the observed low-frequency modes can be difficult. For instance, Balona & Dziembowski (2011) analysed over 12 000 *Kepler* stars and identified 1568 candidate δ Sct pulsators. They defined a group of δ Sct stars with low-frequency modes similar to those characteristic for γ Dor stars. Photometric atmospheric parameters place all of these stars in the γ Dor region of the H–R diagram. Accurate stellar atmospheric parameters are obligatory to place the observed γ Dor/δ Sct hybrids in the H–R diagram.

The investigation of *Kepler* data revealed A- and F-type stars located in the δ Scuti or γ Doradus instability regions but showing no variability (Guzik et al. 2015; Murphy et al. 2015). The simplest explanation of this phenomenon is that the atmospheric parameters are incorrect. If so, the determination of accurate values would place the star outside the instability regions. Other explanations are observational constraints preventing the detection of oscillations with amplitudes below the noise level of the data, or the existence of a physical mechanism that inhibits pulsations for some stars. The problem of non-pulsating A and F stars is widely discussed in Guzik et al. (2015) and Murphy et al. (2015).

The analysis of large samples of A and F stars helps in finding answers to many questions concerning these stars and their atmospheres in general, like the $v \sin i$ distribution and the influence of fast rotation on chemical abundances, the dependence of microturbulent velocity on effective temperature and surface gravity and the reasons for peculiar abundances of chemical elements amongst A and F stars.

This paper is organized as follows. In Section 2, we describe observational data used in the analysis, methods of data reduction, calibration and normalization. The methods applied for spectral classification and for determining the atmospheric parameters of the investigated objects, together with the sources of possible errors, are given in Section 3. The results are discussed in Section 4. The sample of chemically peculiar (CP) stars is discussed in Section 5. Positions of the stars in the log T_{eff}–log g diagram and the discussion of their pulsation properties are shown in Section 6. Conclusions and future prospects are given in Section 7.

2 SPECTROSCOPIC SURVEYS OF *KEPLER* STARS

In this work we analyse the spectra taken with the cross-dispersed, Fibre-Fed Échelle Spectrograph (FIES; Telting et al. 2014), attached to the 2.56-m Nordic Optical Telescope (NOT) located on La Palma (Canary Islands, Spain). The obtained spectra have 'medium' $R \sim 46\,000$ or 'low' $R \sim 25\,000$ resolving power and cover the visual spectral range from 3700 to 7300 Å. Signal-to-noise ratio (S/N) for an individual spectrum at 5500 Å is 80–100.

The spectra have been reduced with a dedicated PYTHON software package FIESTOOL[1] (Telting et al. 2014) based on IRAF.[2] The standard procedures have been applied, which includes bias subtraction, extraction of scattered light produced by the optical system, cosmic ray filtering, division by a normalized flat-field, wavelength calibration by a ThArNe lamp and order merging. Normalization to the continuum was performed using the standard IRAF procedure *continuum*. The accuracy of the normalization was tested by fitting synthetic spectra to four Balmer lines (Hα, Hβ, Hγ and Hδ) in the spectrum of each star. The normalization process was successful if all hydrogen lines can be fitted satisfactorily with the same T_{eff}. Otherwise, the whole procedure is repeated. If several spectra were available for a star, we analysed the averaged spectrum. The averaging process is applied after normalization and forms an additional test of the quality of the normalization process.

The data analysed here were collected during the spectroscopic survey carried out between 2010 and 2012. The stars were selected on the basis of spectral types and photometric atmospheric parameters available in the Kepler Input Catalogue (KIC; Brown et al. 2011) as a potential δ Sct, γ Dor or hybrid variables.

Table 1 lists the stars analysed and gives their KIC numbers, year of the observations, number of spectra and their resolution, visual (*V*) magnitudes and spectral types taken from the literature and determined in the current work. We also provide notes on chemical peculiarity resulting from spectral classification and spectroscopic analysis, type of binarity and pulsation characteristics obtained from *Kepler* data analysis.

3 ATMOSPHERIC PARAMETERS

The basic information about the stars and the initial stellar atmospheric parameters were derived from spectral classification, spectral energy distribution (SED) analysis and taken from the catalogue of Huber et al. (2014, hereafter H2014). Effective temperatures, surface gravities and metallicities determined by these methods were used as input parameters for the high-resolution spectroscopic data analysis. The atmospheric parameters are refined by analysis of the spectral lines, guided by our spectral classifications.

(i) *Spectral classification*. We compared the spectra of the studied stars with those of standards (Gray & Corbally 2009). Our sample consists of A and early F stars, so the spectral type is derived from hydrogen, Ca K and metal lines. For non-CP stars these three sets of lines provide the same spectral type. For CP stars (Am, marginal Am:, λ Boötis) different spectral types are derived. For early A stars the luminosity class is obtained from hydrogen lines, whereas for latter types, the lines of ionized Fe and Ti became useful.

The literature and new spectral classifications of the investigated stars are given in Table 1. The spectral classification process revealed CP stars of Am, Am: and λ Boötis types. Some of these stars were already known peculiar stars (KIC 3429637: Am:, Murphy et al. 2012), (KIC 7767565 and KIC 9828226: Am and λ Boo; Paper I). We classified one new Am: star (KIC 3858884) and two λ Boo objects (KIC 9656348 and KIC 11973705).

Eight stars from our sample were also analysed in Paper I based on the high-resolution HERMES spectra (see Table 1). We took this opportunity to check the influence of spectral resolution, S/N and normalization process on the spectral classification results. No differences in classification were found for KIC 7119530 (A3 IVn) and

---

[1] http://www.not.iac.es/instruments/fies/fiestool/FIEStool.html
[2] Image Reduction and Analysis Facility, http://iraf.noao.edu/

Table 1. Journal of spectroscopic observations, the derived spectral classes and variability classification. *N* is the number of available spectra; SpT1 indicates the spectral classification from the literature, whereas SpT2 means spectral classifications obtained in this work. Additional notations for luminosity class: 'b' – lower luminosity main-sequence star; 'a' or 'a+' – higher luminosity main-sequence star; 'IV-V' – between IV and V; 'IV/V' – either IV or V; 'n' – nebulous (e.g. broad-lined); 's' – sharp lines; 'nn' – very rapid rotators; 'met wk' – weak metal lines; 'met str' – strong metal lines. In the last column additional information taken from spectra and *Kepler* data are presented. 'SB2' means double-lined spectroscopic binary; 'EB' – eclipsing binary; 'ell. var.' – ellipsoidal variable; 'hybrid' – frequencies of γ Dor and δ Sct visible in periodogram; 'HADS' – high amplitude δ Sct variable; 'cont.' – *Kepler* data contaminated by a nearby star; 'unknown' – unknown variability type.

KIC number	Obs. year	N	Resolving power	V (mag)	SpT1 (literature)	SpT2 (this work)	Notes
KIC 2162283	2010	1	Med	9.47	F2[a]	Am+F	EB, ell. var., δ Sct
KIC 2694337	2010	1	Low	10.35	F0.5 IVs[f]	A9 (met str F3)	γ Dor/δ Sct hybrid
KIC 3217554	2010	1	Med	9.56	A5[a]	A3 IVn	SB2, γ Dor (γ Dor/δ Sct hybrid?), cont.
KIC 3219256	2010	1	Med	8.31	A8 V[b]	A9 V	γ Dor/δ Sc hybrid
KIC 3331147	2011	1	Med	10.06	–	F0.5 Vs	γ Dor
KIC 3429637	2010	2	Med	7.72	kF2 hA9 mF3[c], F0 III[b]	kF0 hA8 mF0 IIIas	δ Sct (γ Dor/δ Sct hybrid?)
KIC 3453494	2010	1	Med	9.53	A7 IV[d]	A4 Vn	γ Dor/δ Sct hybrid
KIC 3858884	2010	2	Med	9.28	F5[e]	kA8 hF0 mF2.5 III Am:	SB2, EB, δ Sct
KIC 3868420	2011	1	Med	9.88	–	A9 Vs (Ca wk A4)	HADS (γ Dor/δ Sct hybrid?)
KIC 4647763	2012	2	Low	10.89	–	F0.5 IV-III	δ Sct/γ Dor hybrid
KIC 4840675	2010	1	Med	9.66	F0 Vn[m]	F0 Vn	SB2, δ Sct/γ Dor hybrid
KIC 5641711	2010	2	Low	10.51	F0[a]	F0 Vn	SB2, δ Sct/γ Dor hybrid
KIC 5880360	2010	1	Med	8.75	A0[a]	A3 IVan	unknown (γ Dor?), $0 - 7$ c/d
KIC 5988140	2010	1	Med	8.81	A8 IIIs[f]	A9 IV	δ Sct
KIC 6123324	2010	1	Med	8.71	F0[a]	F2.5 Vn	δ Sct/γ Dor hybrid?
KIC 6279848	2010	1	Med	9.23	F0[a]	F1.5 IVs (met wk A9)	δ Sct/γ Dor hybrid
KIC 6370489	2011	1	Med	8.79	F8 V[g]	F5.5 V	solar-like oscillations
KIC 6443122	2011	1	Med	11.10	–	F0 IVs	δ Sct/γ Dor hybrid
KIC 6670742	2010	1	Med	9.10	A5[a]	F0 Vnn (met wk A7)	δ Sct/γ Dor hybrid
KIC 7119530	2010	1	Med	8.44	A3 IVn[f]	A3 IVn	δ Sct/γ Dor hybrid
KIC 7122746	2012	2	Low	10.62	–	A5 Vn	δ Sct/γ Dor hybrid?
KIC 7668791	2010	1	Med	9.21	A2[a]	A5/7 IV/V	δ Sct
KIC 7748238	2011	1	Med	9.54	A9.5 V-IV[d]	F1 V (met wk F0)	δ Sct/γ Dor hybrid
KIC 7767565	2010	1	Med	9.29	kA5 hA7 mF1 IV Am[f]	kA5 hA7 mF1 IV Am	γ Dor
KIC 7773133	2012	1	Low	10.93	–	F0 IIIas	δ Sct (δ Sct/γ Dor hybrid?)
KIC 7798339	2010	1	Med	7.85	F3 IV[b]	F1.5 IV	γ Dor
KIC 8211500	2010	1	Med	8.08	A5 IV[h]	A6 V	Unknown (γ Dor?)
KIC 8222685	2010	1	Med	8.89	F0 V[i]	F0 V	γ Dor
KIC 8694723	2011	1	Med	8.92	G0 IV[g]	hF6 mF2 gF5 V	solar-like oscillations
KIC 8827821	2012	1	Low	11.14	–	A8 IV-V	δ Sct/γ Dor hybrid?
KIC 8881697	2010	1	Low	10.50	A5[i]	A8 Vn	δ Sct/γ Dor hybrid
KIC 8975515	2010	1	Med	9.48	A6 V:[f]	A7 IV	SB2, δ Sct/γ Dor hybrid
KIC 9229318	2010	1	Med	9.59	F0[a]	A8 III (met str F0)	δ Sct/γ Dor hybrid
KIC 9349245	2010	1	Med	8.11	Am:[j]	F2 IIIs	Constant
KIC 9408694	2011	2	Med	11.48	–	F0 IVs + ?	HADS (δ Sct/γ Dor hybrid?)
KIC 9410862	2012	2	Low	10.78	–	F6 V	Solar-like oscillations
KIC 9650390	2010	1	Med	9.32	A0[a]	A3 IV-Vnn (met wk A2.5)	δ Sct/γ Dor hybrid
KIC 9655114	2010	1	Low	12.03	A4[k]	A5 Vn	SB2, δ Sct + cont.
KIC 9656348	2010	3	Low	10.28	–	hA9 kA4m A4 V λ Boo	δ Sct/γ Dor hybrid
KIC 9828226	2012	1	Low	9.92	hA2 kA0 mB9 Vb[f]	hA2 kB9.5 mB9 Vb λ Boo	δ Sct/γ Dor hybrid
KIC 9845907	2012	3	Low	11.42	–	A4 IVs	δ Sct
KIC 9941662	2011	1	Med	9.95	A0[a]	kA2 hA5 mA7 (IV) Am:	Constant, planet transit
KIC 9970568	2010	1	Med	9.58	A4 IVn[f]	A8 Vnn (met wk A4)	δ Sct/γ Dor hybrid
KIC 10030943	2011	2	Med	11.45	–	F1.5 IV-V	ell. var., δ Sct
KIC 10341072	2010	1	Med	8.95	F8[a]	F6 III	Unknown
KIC 10661783	2011	1	Med	9.53	A2[a]	A5 IV	EB, δ Sct
KIC 10717871	2012	1	Low	10.52	–	F0 V	γ Dor/δ Sct hybrid
KIC 11044547	2012	1	Low	9.94	A0[a]	A2 Vs	δ Sct (δ Sct/γ Dor hybrid?)
KIC 11622328	2010	1	Med	9.42	A2[a]	A4.5 Vn	Unknown (γ Dor?)
KIC 11973705	2010	1	Med	9.09	B8.5IV-V[l]	hF0.5 kA2.5m A2.5 V λ Boo	ell. var., δ Sct/γ Dor hybrid

Note. [a]Heckmann & Dieckvoss (1975); [b]Catanzaro et al. (2011); [c]Abt (1984); [d]Tkachenko et al. (2012); [e]Kharchenko (2001); [f]Paper I; [g]Molenda-Żakowicz et al. (2013); [h]Murphy et al. (2015); [i]Macrae (1952); [j]Catanzaro et al. (2015); [k]Lindoff (1972); [l]Lehmann et al. (2011); [m]and this work.
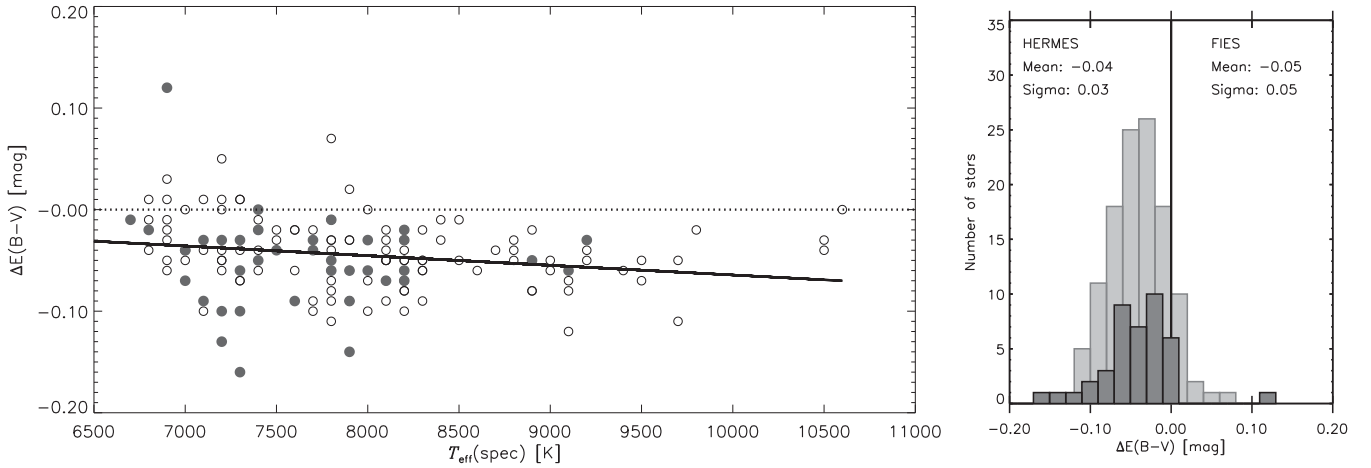
Figure 1. Left-hand panel: the differences $\Delta E(B - V) = E(B - V)(\text{Na}) - E(B - V)(\text{KIC})$ as a function of $T_{\text{eff}}(\text{FE})$. A linear function is fitted (solid line). The open circles represent results taken from Paper I. The filled circles indicate the results obtained here. Right-hand panel: the distribution of differences $\Delta E(B - V)$ for Paper I stars (HERMES observations, light grey histogram) and objects analysed here (FIES observations, dark grey histogram). Arithmetic means and standard deviations of both distributions are indicated in the figure.

CP stars KIC 7767565 (kA5 hA7 mF1 IV Am) and KIC 9828226 (hA2 kA0 mB9 Vb and hA2 kB9.5 mB9 Vb, the negligible difference in spectral type from Ca lines). Minor differences not more than one temperature subclass or one luminosity class were found for KIC 5988140 (A8 IIIs and A9 IV), KIC 8975515 (A6 V: and A7 IV) and KIC 2694337 (F0.5 IVs and A9 met strong F3). Larger differences were found for the very fast rotating star KIC 9970568 (A4 IVn and A8 Vnn met wk A4). This could be a consequence of differences in the normalization of the broad, blended spectral lines.

(ii) *Interstellar reddening*. SEDs are affected by interstellar reddening $E(B - V)$. Therefore, we estimated this parameter using the equivalent width of the interstellar Na D_2 (5889.95 Å) line. $E(B - V)$ values were obtained from the relation given by Munari & Zwitter (1997). The equivalent widths of the individual components were measured for those with resolved multicomponent interstellar Na D_2 lines. Because the interstellar reddening is additive (Munari & Zwitter 1997), the total $E(B - V)$ is the sum of the reddening per component.

In Fig. 1, the spectroscopic interstellar reddenings $E(B - V)(\text{Na})$ were compared with $E(B - V)$ values from the KIC catalogue, $E(B - V)(\text{KIC})$, for stars analysed here and those taken from Paper I. The current results fully confirm those obtained in Paper I. The photometric interstellar reddenings given in the KIC are higher than $E(B - V)(\text{Na})$ and the differences increase with effective temperature. The highest differences between $E(B - V)(\text{Na})$ and $E(B - V)(\text{KIC})$ were obtained for faint stars (KIC 10030943, KIC 6443122, KIC 9408694 and KIC 9845907).

(iii) *Spectral energy distributions*. Stellar effective temperatures T_{eff} were determined from SEDs, constructed from the available photometry and TD-1 ultraviolet fluxes (Carnochan 1979). For photometric data we searched the same photometric catalogues as in Paper I. The constructed SEDs were de-reddened using the appropriate analytical extinction fits of Seaton (1979) and Howarth (1983) for the ultraviolet and the optical and infrared spectral ranges, respectively.

As in Paper I, we obtained T_{eff} values using a non-linear least-squares fit to the SED. We fixed $\log g = 4.0$ and [M/H] = 0.0 for all of the stars, since they are poorly constrained by the SED. The results are given in Table 2. The uncertainties in T_{eff} include the formal least-squares error and those due to the assumed uncertainties in

$E(B - V)$ of ± 0.02 mag, $\log g$ of ± 0.5 and [M/H] of ± 0.5 dex. The latter two were included to assess the effect of the assumed fixed values $\log g$ and [M/H] on the T_{eff} obtained from the SED. The four individual contributions to the uncertainties in T_{eff} were added in quadrature, but overall uncertainty is mostly dominated by the formal least-squares error.

(iv) *Balmer lines*. The values of T_{eff} were obtained using the sensitivity of Balmer lines to this parameter, following the method proposed by Catanzaro, Leone & Dall (2004). On the other hand, hydrogen lines are not good indicators of $\log g$ for effective temperatures lower than about 8000 K. Therefore, for almost all stars but two (KIC 9828226 and KIC 11044547), the initial surface gravity was assumed to be equal to 4.0 dex. We used an iterative approach to minimize the differences between observed and theoretical Hδ, Hγ and Hβ profiles (see Catanzaro et al. 2004). The effective temperature obtained from the Balmer lines was then revisited when a $\log g$ value from the Fe lines was available.

The uncertainties in $\log g$ and continuum placement were accounted for when estimating the uncertainty in the derived values. First, we take into account the differences in the determined T_{eff} values from separate Balmer lines. Next, we check the influence of the assumed $\log g$ value on the final T_{eff} value. For most stars, the obtained uncertainties equal 100 K (this is the step of T_{eff} in the grid of synthetic fluxes). The bigger errors are caused by incorrect normalization (see Table 2).

(v) *Iron lines*. The atmospheric parameters, chemical compositions and $v \sin i$ were determined through the analysis of lines of neutral and ionized iron. In general, we required that the abundances obtained from Fe I and Fe II lines yield the same result. The detailed analysis of the iron lines was fully discussed in Paper I. In brief, we proceeded according to the following scheme: microturbulence ξ_t was adjusted until there was no correlation between iron abundances and line depths for the Fe I lines; T_{eff} was changed until there was no trend in the abundance versus excitation potential for the Fe I lines and $\log g$ was obtained by requiring the same Fe abundance from the lines of both Fe II and Fe I ions.

For hotter stars, with more Fe II than Fe I lines visible in the spectra, the Fe II lines were used to determine T_{eff} and ξ_t. This approach is limited by stellar rotation, since line blending grows rapidly with $v \sin i$. In cases where the analysis of individual lines

Table 2. Atmospheric parameters of the investigated *Kepler* A- and F-type stars. Photometric values (H2014 and KIC), those obtained from spectral energy distributions (Na and SED) and from analysis of metal and Balmer lines are presented. The 1σ uncertainties are given for effective temperatures from SED and for $v\sin i$ and $\log \epsilon(Fe)$ values from metal lines.

KIC number	H2014 and KIC T_{eff} (K)	$\log g$	$E(B-V)$ (mag)	$\log \epsilon(Fe)$	Na D and SED $E(B-V)$ (mag)	T_{eff} (K)	Balmer lines T_{eff} (K)	T_{eff} (K)	Fe lines $\log g$	ξ_t (km s^{-1})	$v\sin i$ (km s^{-1})	$\log \epsilon(Fe)$
2162283	6947	4.07	0.05	7.60	0.01	7030 ± 150	7100 ± 100	7000 ± 100	4.1 ± 0.1	3.1 ± 0.1	42 ± 2	7.70 ± 0.14
2694337	7526	3.96	0.08	7.42	0.06	7640 ± 190	7300 ± 100	7400 ± 100	4.1 ± 0.1	3.0 ± 0.1	96 ± 3	7.60 ± 0.07
3219256	7493	3.59	0.06	7.48	0.03	7550 ± 180	7500 ± 100	7300 ± 100	3.8 ± 0.1	3.0 ± 0.1	99 ± 3	7.40 ± 0.10
3331147	7256	3.60	0.10	7.28	0.03	7040 ± 150	7000 ± 100	7000 ± 100	3.7 ± 0.1	2.0 ± 0.1	63 ± 2	7.46 ± 0.13
3429637	7211	3.99	0.12	7.30	0.02	7260 ± 160	7200 ± 100	7300 ± 100	3.4 ± 0.1	2.9 ± 0.1	51 ± 1	7.55 ± 0.08
3453494	7766	3.64	0.09	7.38	0.03	7830 ± 200	7800 ± 100	8000 ± 200	3.8 ± 0.2	2.0 ± 0.4	230 ± 9	7.42 ± 0.11
3868420	6782	4.08	0.06	7.24	0.00	6090 ± 110	7600 ± 200	7800 ± 100	3.9 ± 0.1	2.9 ± 0.1	11 ± 1	7.93 ± 0.13
4647763	6842	3.52	0.08	7.44	0.05	7220 ± 170	7100 ± 100	7100 ± 100	3.8 ± 0.1	3.9 ± 0.1	69 ± 2	7.39 ± 0.08
5880360	7930	3.68	0.08	7.34	0.05	8070 ± 220	7900 ± 100	7700 ± 200	3.6 ± 0.2	3.5 ± 0.3	187 ± 10	7.18 ± 0.13
5988140	7404	3.28	0.09	7.57	0.04	7630 ± 180	7800 ± 200	7800 ± 100	3.8 ± 0.1	1.9 ± 0.1	52 ± 2	7.48 ± 0.11
6123324	6691	3.09	0.07	7.57	0.05	7110 ± 160	7000 ± 100	6800 ± 200	3.5 ± 0.2	3.9 ± 0.3	189 ± 18	6.63 ± 0.18
6279848	6843	3.75	–	7.64	0.03	7000 ± 150	7000 ± 200	7100 ± 100	4.0 ± 0.1	3.2 ± 0.1	39 ± 1	7.27 ± 0.09
6370489	6302	3.92	0.02	7.30	0.01	6300 ± 120	6200 ± 100	6300 ± 100	4.0 ± 0.1	1.4 ± 0.1	7 ± 1	7.12 ± 0.12
6443122	7696	3.54	0.17	6.92	0.04	7420 ± 190	7100 ± 100	7200 ± 100	3.8 ± 0.1	3.0 ± 0.1	83 ± 3	7.50 ± 0.08
6670742	7694	3.63	0.08	7.42	0.02	7540 ± 190	7400 ± 100	7300 ± 200	3.6 ± 0.2	3.2 ± 0.4	276 ± 8	7.31 ± 0.11
7119530	7521	3.26	0.09	7.57	0.07	8240 ± 230	7800 ± 100	8200 ± 200	3.8 ± 0.2	2.5 ± 0.4	240 ± 11	7.35 ± 0.21
7122746	7710	4.00	0.15	7.56	0.08	8390 ± 280	8200 ± 100	8100 ± 100	4.1 ± 0.2	2.9 ± 0.2	110 ± 5	7.46 ± 0.12
7668791	8394	3.78	0.08	7.28	0.02	8110 ± 220	8200 ± 100	8200 ± 100	3.8 ± 0.1	2.7 ± 0.1	51 ± 2	7.46 ± 0.10
7748238	7244	4.06	0.10	7.32	0.05	7440 ± 170	7200 ± 100	7400 ± 100	3.9 ± 0.2	3.0 ± 0.2	129 ± 4	7.48 ± 0.11
7767565	8466	3.98	–	7.71	0.06	7810 ± 200	7900 ± 200	7800 ± 100	3.8 ± 0.1	2.7 ± 0.1	62 ± 3	7.75 ± 0.13
7773133	6977	3.53	0.13	7.30	0.10	7070 ± 170	7100 ± 100	7200 ± 100	3.9 ± 0.1	2.9 ± 0.1	41 ± 2	7.64 ± 0.11
7798339	6878	3.91	0.05	7.44	0.01	7000 ± 150	6800 ± 100	7000 ± 100	3.9 ± 0.1	2.5 ± 0.1	13 ± 1	7.13 ± 0.12
8211500	7619	3.93	0.04	7.60	0.01	7730 ± 180	7900 ± 100	8000 ± 100	3.9 ± 0.1	2.4 ± 0.1	90 ± 7	7.56 ± 0.09
8222685	6861	4.17	–	7.60	0.01	7150 ± 160	7100 ± 100	7100 ± 100	3.8 ± 0.1	3.2 ± 0.1	82 ± 2	7.20 ± 0.07
8694723	6120	4.10	0.03	6.91	0.02	6370 ± 120	6100 ± 100	6200 ± 100	4.1 ± 0.1	1.3 ± 0.1	7 ± 1	7.02 ± 0.10
8827821	7610	3.71	0.14	7.50	0.10	7680 ± 190	7400 ± 100	7700 ± 100	3.7 ± 0.1	3.4 ± 0.1	87 ± 2	7.60 ± 0.07
8881697	7932	3.93	0.11	7.40	0.05	7800 ± 200	7700 ± 100	7900 ± 200	3.8 ± 0.2	3.3 ± 0.3	184 ± 4	7.51 ± 0.11
9229318	7358	3.63	0.09	7.38	0.09	7550 ± 180	7200 ± 100	7400 ± 100	4.0 ± 0.1	3.0 ± 0.1	66 ± 2	7.74 ± 0.08
9349245	7914	3.72	0.05	7.06	0.02	7880 ± 210	8000 ± 200	8200 ± 100	3.7 ± 0.1	2.9 ± 0.1	82 ± 2	7.92 ± 0.11
9408694	6813	3.78	0.16	7.42	0.00	7120 ± 170	7200 ± 100	7300 ± 100	4.0 ± 0.1	2.0 ± 0.1	16 ± 1	7.53 ± 0.13
9410862	6230	4.32	0.04	7.30	0.04	6240 ± 130	6000 ± 100	6100 ± 100	3.9 ± 0.1	1.3 ± 0.1	4 ± 1	7.18 ± 0.13
9650390	8572	3.77	0.10	7.30	0.05	8510 ± 290	8100 ± 200	8900 ± 200	3.9 ± 0.2	3.2 ± 0.4	267 ± 7	7.63 ± 0.11
9656348	7177	3.90	0.14	7.57	0.05	7600 ± 180	7400 ± 200	7600 ± 100	3.9 ± 0.1	3.0 ± 0.1	32 ± 2	6.83 ± 0.11
9828226	9155	4.03	0.10	7.57	0.04	8950 ± 370	9000 ± 200	9100 ± 100	4.1 ± 0.1	2.0 ± 0.1	99 ± 18	6.39 ± 0.21
9845907	8148	4.01	0.14	7.57	0.00	7540 ± 220	7900 ± 200	7900 ± 100	3.9 ± 0.1	2.0 ± 0.1	13 ± 1	7.10 ± 0.11
9941662	9107	3.87	0.10	7.57	0.03	6940 ± 140	8100 ± 100	8200 ± 100	4.1 ± 0.1	2.7 ± 0.1	76 ± 3	7.65 ± 0.06
9970568	8035	3.71	0.11	7.40	0.10	8080 ± 220	7800 ± 100	7800 ± 200	4.0 ± 0.2	2.1 ± 0.4	250 ± 11	7.35 ± 0.09
10030943	6883	4.23	0.07	7.64	0.19	7410 ± 210	6900 ± 100	6900 ± 100	4.0 ± 0.1	3.8 ± 0.1	79 ± 4	7.07 ± 0.10
10341072	6543	4.17	0.03	7.38	0.02	6610 ± 130	6700 ± 300	6700 ± 100	3.8 ± 0.2	3.0 ± 0.2	104 ± 2	7.65 ± 0.08
10661783	8117	3.72	0.10	7.34	0.01	7960 ± 220	7800 ± 100	7900 ± 100	4.1 ± 0.1	1.8 ± 0.1	83 ± 2	7.51 ± 0.12
10717871	7485	3.51	0.12	7.57	0.03	7200 ± 160	7200 ± 100	7100 ± 100	3.9 ± 0.2	2.0 ± 0.2	128 ± 5	7.45 ± 0.11
11044547	9143	3.89	0.11	7.57	0.08	9360 ± 470	9000 ± 200	9200 ± 100	4.0 ± 0.1	1.2 ± 0.1	68 ± 4	7.60 ± 0.13
11622328	7725	4.19	–	7.57	0.06	8250 ± 240	8300 ± 300	8300 ± 100	3.8 ± 0.2	2.8 ± 0.2	144 ± 5	7.41 ± 0.09
11973705	11086	3.98	0.05	7.57	0.01	7520 ± 180	7400 ± 100	7500 ± 100	3.9 ± 0.2	3.4 ± 0.2	114 ± 7	6.52 ± 0.14

Note. Results using TD-1: KIC 3219256: 7750 ± 290 K; KIC 3429637: 7340 ± 330 K; KIC 7119530: 8380 ± 220 K; KIC 7668791: 8580 ± 240 K; KIC 7798339: 7110 ± 290 K; KIC 8211500: 8040 ± 290 K; KIC 9349245: 8030 ± 200 K; KIC 9650390: 8870 ± 240 K.

Comments on individual stars:

KIC 3868420 (WDS 19434+3855): 10.35 + 10.61 mag pair, separation 2.5 arcsec plus wide (26 arcsec) 11.71 mag companion. 2MASS photometry is unreliable. Some available photometry is for the individual stars (e.g. Tycho) but other is for the combined light of the close pair. Insufficient photometry of the individual stars to obtain SED fits for each star. HADS pulsator, so photometry will sample star at different phases and brightnesses.

KIC 7767565 (WDS 19457+4330): close pair 9.50+10.0 mag, separation 0.3 arcsec. Results for combined light.

KIC 8211500 (WDS 18462+4408): 8.19+11.28 mag, separation 0.7 arcsec. Results for combined light, but large magnitude difference means that the faint companion should not affect the results.

KIC 9408694 (V2367 Cyg): HADS pulsator, so photometry will sample star at different phases and brightnesses.

KIC 9941662 (Kepler-13, WDS 19079+4652): 10.35+10.48 mag, pair separation 1.1 arcsec. Photometry is for combined light of the pair. Literature shows that both stars have similar magnitudes to within 0.1 ~ 0.2 mag. SED fit may represent the average of the two stars, but not the individual stars. Fits are therefore not considered reliable.

was impossible we assumed that the iron abundances obtained from different spectral regions are the same for the correct T_{eff}, log g and ξ_{t} values. The analysis relies on the same physics, regardless of rotation (see Paper I for further explanation).

We analysed the metal lines using spectrum synthesis, relying on an efficient least-squares optimization algorithm (see Paper I). The chosen method allows for a simultaneous determination of various parameters influencing stellar spectra. The synthetic spectrum depends on T_{eff}, log g, ξ_{t}, $v\sin i$ and the relative abundances of the elements. Due to the fact that all atmospheric parameters are correlated, the T_{eff}, log g and ξ_{t} parameters were obtained prior to the determination of chemical abundances. The remaining parameters (chemical abundances and $v\sin i$) were determined simultaneously. The $v\sin i$ values were determined by comparing the shapes of observed metal line profiles with the computed profiles, as shown by Gray (2005). Chemical abundances and $v\sin i$ values were determined from many different lines or regions of the spectrum. In the final step of the analysis, we derived the average values of $v\sin i$ and abundances of all the chemical elements considered for a given star.

We used atmospheric models (plane–parallel, hydrostatic and radiative equilibrium) and synthetic spectra computed with the line-blanketed, local thermodynamical equilibrium (LTE) code ATLAS9 (Kurucz 1993a). The grid of models was calculated for effective temperatures between 5000 and 12 000 K with a step of 100 K, surface gravities from 2.0 to 4.6 dex with a step of 0.1 dex, microturbulence velocities between 0.0 and 6.0 km s^{-1} with a step of 0.1 km s^{-1} and for metallicities of 0.0, -0.5 and -1.0. The synthetic spectra were computed with the SYNTHE code (Kurucz 1993b). Both codes, ATLAS9 and SYNTHE, were ported to GNU/Linux by Sbordone (2005) and are available online.[3] We used the line list of Castelli & Hubrig (2004). In our method we take into account all elements that show lines in the chosen spectral region. Elements with little or no influence are assumed to have solar abundances or abundances typical for the analysed star. The stellar rotation and S/N of the spectrum dictate which elements will be analysed. The atmospheric parameters obtained from our analysis are given in Table 2, and the abundances of analysed elements are given in Table B1.

The derived atmospheric parameters and chemical abundances are influenced by errors from a number of sources. Several assumptions, e.g., plane parallel geometry (1-D), and hydrostatic equilibrium (Kurucz 1993a), made in the atmosphere models used to compute the synthetic spectra; adopted atomic data (see Kurucz 2011); non-LTE effects for Fe I and Fe II lines (see Mashonkina 2011). These error sources have already been discussed in Paper I.

The quality (resolution, S/N) and wavelength range of the observed spectra, as well as their normalisation can influence the results. The difficulty of normalisation increases for heavily blended spectra of stars with $v\sin i$ higher than about 100 km s^{-1}, even for high-resolution and high S/N data. This problem was also discussed by Ryabchikova et al. (2016) and Kahraman Aliçavuş et al. (2016). For a few stars we have FIES and HERMES spectra at our disposal. The HERMES data were analysed in the Paper I. The S/N of the data is similar, but the resolution differs significantly. The HERMES spectra have a resolving power of about 90 000, compared to 24 000 (low resolution) or 46 000 (medium resolution) for FIES. Both HERMES and FIES spectra are available for KIC 2694337, KIC 9828226 (low resolution FIES spectra) and KIC 4840675 (SB2), KIC 5988140, KIC 7119530, KIC 7767565, KIC 8975515 (SB2) and KIC 9970568 (medium resolution FIES spectra).

For these stars we can compare the results obtained from different sets of spectra. We found that the differences in T_{eff} and log g do not exceed 100 K and 0.1 dex, respectively. The biggest differences in ξ_{t} were obtained for KIC 2694337 (0.4 km s^{-1}), KIC 7119530 (0.6 km s^{-1}), and KIC 9970568 (0.3 km s^{-1}; but in agreement within the error bars). This is due to the effect of different lines used for analysis. For the other stars the discrepancies were no more than 0.1 km s^{-1}. Both Ryabchikova et al. (2016) and Kahraman Aliçavuş et al. (2016) obtained similar results.

The chemical abundances are affected by uncertainties in atmospheric parameters. For example, an error of T_{eff} equal to 100 K leads to changes in abundances smaller than 0.1 dex in most cases. Similarly, an error of log g equal to 0.1 dex changes chemical abundances by about 0.05 dex, and a 0.1 km s^{-1} uncertainty in ξ_{t} changes abundances by no more than 0.15 dex. The uncertainty of the microturbulence velocity increases with $v\sin i$, from 0.1 km s^{-1} for small and moderate velocities to 0.4 km s^{-1} for rapid rotators. Chemical abundances determined for rapidly rotating stars have the largest uncertainty. The combined errors of chemical abundances were calculated as in Paper I. In most cases these errors are lower than 0.20 dex. The $v\sin i$ values obtained from HERMES and FIES spectra are consistent.

4 DISCUSSION OF THE RESULTS

4.1 Atmospheric parameters

Here we discuss the consistency of our atmospheric parameters from the FIES spectra with those from two other sources: the H2014 catalogue and SEDs. The $v\sin i$ values are compared with typical values for A and F stars. All parameters are presented in the Table 2.

4.1.1 Effective temperature

The effective temperatures given by H2014 and determined using the methods described in Section 3 are presented in Table 2 and compared in Fig. 2. In this figure, the differences between T_{eff}(FE) obtained from the analysis of the high-resolution spectra and values taken from H2014, T_{eff}(H2014), from SED fitting, T_{eff}(SED), and from the Balmer lines analysis, T_{eff}(Balmer), are shown as a function of T_{eff}(FE). The biggest differences are for T_{eff}(H2014) values. The H2014 catalogue is a compilation of literature values for atmospheric properties (T_{eff}, log g and [Fe/H]) derived from different methods, including photometry, spectroscopy, asteroseismology and exoplanet transits. For the stars considered here, the H2014 values have been determined with large uncertainties via photometry. For most of the stars, the values of T_{eff}(FE) $- T_{\mathrm{eff}}$(H2014) agree to within $\pm$300 K. The biggest differences are obtained for CP stars KIC 3868420 (Am star from high-resolution spectra analysis; HADS pulsator), KIC 7767565 (Am), KIC 9941662 (Am:) and KIC 11973705 (λ Boo), and for rapidly rotating stars with $v\sin i$ exceeding 100 km s^{-1}, e.g. KIC 11622328 and KIC 7119530.

Fig. 2(b) compares T_{eff}(FE) with T_{eff}(SED). The consistency between the results of these two methods is good. To compare the effective temperatures obtained with different methods we use the Kendall's rank correlation coefficient that measures the strength of dependence between two variables. There is no significant trend of the differences [T_{eff}(FE) $- T_{\mathrm{eff}}$(SED)] with T_{eff}(FE). The Kendall's rank correlation coefficient is 0.16. The differences exceed 500 K
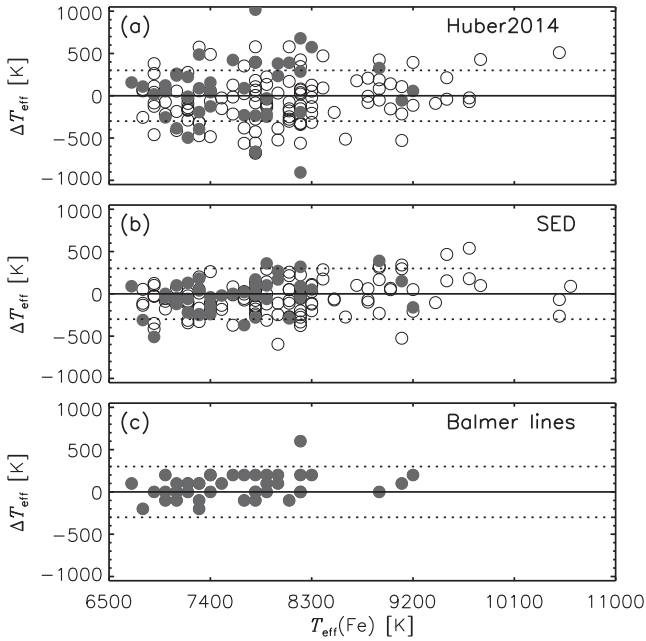
Figure 2. Comparison of effective temperatures derived by different methods. Filled circles represent the results obtained in this work, open circles are used for Paper I stars. In panel (a) the differences $\Delta T_{\mathrm{eff}} = T_{\mathrm{eff}}(\mathrm{Fe}) - T_{\mathrm{eff}}(\mathrm{H2014})$ are shown. In panel (b) $\Delta T_{\mathrm{eff}} = T_{\mathrm{eff}}(\mathrm{Fe}) - T_{\mathrm{eff}}(\mathrm{SED})$ are plotted. In panel (c) $\Delta T_{\mathrm{eff}} = T_{\mathrm{eff}}(\mathrm{Fe}) - T_{\mathrm{eff}}(\mathrm{Balmer})$ are shown.

only for KIC 10030943 and KIC 9941662. KIC 10030943 is an eclipsing binary star. The difference $T_{\mathrm{eff}}(\mathrm{Fe}) - T_{\mathrm{eff}}(\mathrm{SED})$ may be the result of the influence of the secondary star on the photometric indices and/or on the spectrum. KIC 9941662 (Kepler-13) is also a binary system, with a magnitude difference $\Delta m = 0.13$ and 1.1 arcsec separation. The photometry used to construct the SED is the combined light of the pair. The $T_{\mathrm{eff}}(\mathrm{SED})$ analysis supports the claimed accuracy of our spectroscopic temperatures because the stars are similar.

The differences $T_{\mathrm{eff}}(\mathrm{Fe}) - T_{\mathrm{eff}}(\mathrm{Balmer})$ are in all cases smaller than 300 K (see Fig. 2c).

4.1.2 Surface gravities

Fig. 3 compares the $\log g(\mathrm{Fe})$ values obtained from high-resolution HERMES (open circles, Paper I) and FIES (filled circles, this work) spectroscopy with those taken from the H2014 catalogue, $\log g(\mathrm{H2014})$. For most stars the surface gravities are consistent to within ± 0.2 dex. There is no correlation between the differences $[\log g(\mathrm{Fe}) - \log g(\mathrm{H2014})]$ and effective temperature or surface gravity. The values in the H2014 catalogue were mostly calculated from photometry. The high-resolution spectra are much more sensitive to $\log g$ than the photometric indices. Therefore, the spectroscopic surface gravities determined from iron lines should be adopted for the subsequent analysis of these stars.

4.1.3 Microturbulent velocity

One of the important key parameters in the abundance analysis is microturbulence ξ_{t}. Microturbulent velocity originates from non-thermal velocities in the stellar atmosphere at scales shorter than the
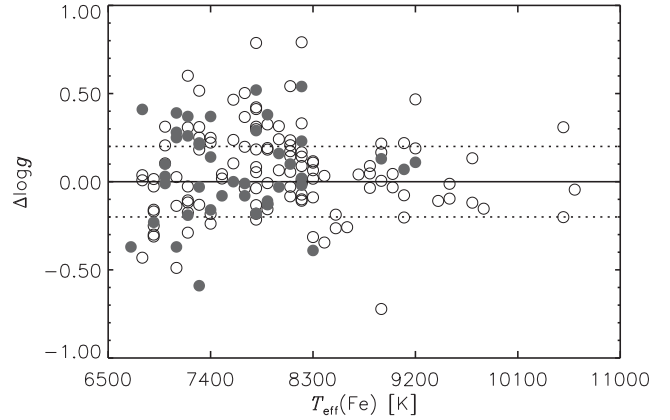

Figure 3. Differences $\Delta \log g = \log g(\mathrm{Fe}) - \log g(\mathrm{H2014})$ as a function of $T_{\mathrm{eff}}(\mathrm{Fe})$. The stars indicated by open circles are taken from Paper I. The filled circles show the results obtained in this work. The dotted horizontal lines indicate a difference of ± 0.2 dex.

mean free path of a photon. It has a significant effect on the spectral lines of A and F stars, therefore its determination is important in abundance analyses, especially when using strong line features.

The microturbulent velocities obtained in our analyses lie within the range from about 1.2 to 3.9 km s^{-1}. Microturbulent velocities are calculated using Fe lines of various strengths, leading to a dependence on spectral quality. The best data are characterized by a high S/N and high resolution. Low S/N and/or resolution prevents weak lines from being analysed. Additionally, the precision of the calculated ξ_{t} values depends strongly on $v\sin i$. At high $v\sin i$, line blending obscures weak lines. The uncertainties of ξ_{t} listed in Table 2 increase with the increasing $v\sin i$ value.

To enlarge the sample, the results from Paper I and Kahraman Aliçavuş et al. (2016) were taken into account. The authors of Paper I analysed stars with a broad range of $v\sin i$ values and found ξ_{t} within the range 2–4 km s^{-1} for stars with $7000 < T_{\mathrm{eff}} \leq 8000$ K, decreasing to 2 km s^{-1} at $8000 < T_{\mathrm{eff}} \leq 9000$ K and decreasing further to 0.5–1 km s^{-1} for $T_{\mathrm{eff}} > 9000$ K. With a larger sample of stars analysed in a consistent way, we re-examine the dependence of ξ_{t} on T_{eff}, $\log g$ and the influence of $v\sin i$ and chemical composition on the determined values.

The absence of a correlation between ξ_{t} and $v\sin i$ (Fig. 4) shows that microturbulence is still well determined across a wide range of $v\sin i$ despite the aforementioned challenges, and that there is no physical connection between the quantities, unless that connection is anticorrelated with a systematic misestimation. There is also no correlation of ξ_{t} and iron abundance; however, the analysed objects fall within a narrow range of iron abundances, in which most stars have $\log \epsilon(\mathrm{Fe})$ between about 7.0 and 8.0.

In Fig. 5 the microturbulences are shown as a function of effective temperature. Here, a broad maximum in ξ_{t} is observed around 7000–8500 K. These results are consistent with the previous determinations of microturbulence for A and F stars. Chaffee (1970) first found that microturbulence varies with effective temperature, from 2 km s^{-1} for early A stars up to 4 km s^{-1} for late A stars, and 2 km s^{-1} for mid F stars. Since then the dependence of ξ_{t} with T_{eff} has been investigated in many studies (Coupry & Burkhart 1992; Edvardsson et al. 1993; Gray, Graham & Hoyt 2001; Smalley 2004; Takeda et al. 2008; Gebran et al. 2014; Paper I). The large dispersion in the results was found in all mentioned works except in Takeda et al. (2008).
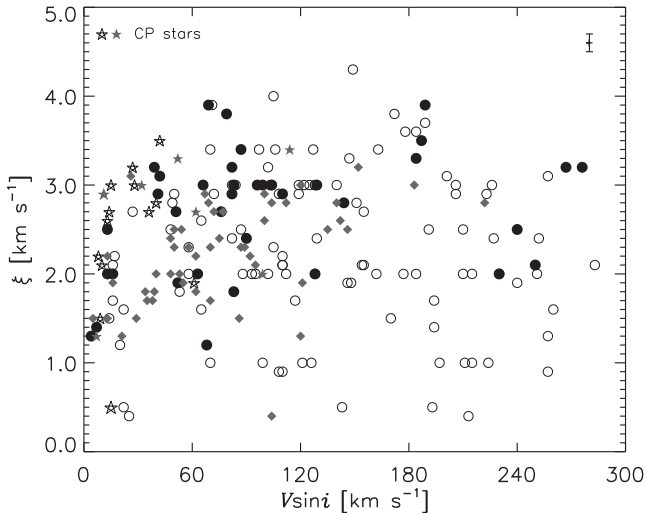
Figure 4. Microturbulent velocities as a function of the projected rotational velocity. The CP stars from Paper I are shown as open stars, whereas the non-CP stars are indicated as open circles. The CP and non-CP objects from this work are presented as filled stars and circles, respectively. Diamonds show results from Kahraman Aliçavuş et al. (2016). Although microturbulence shows no dependence on $v\sin i$, it is determined to higher precision in slow rotators.
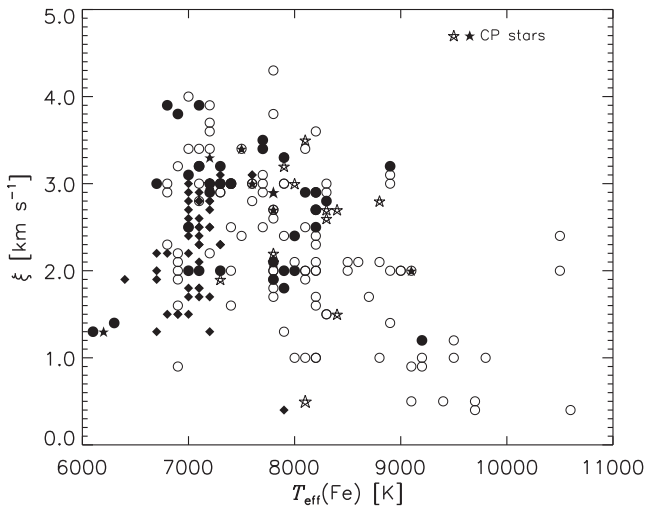

Figure 5. Microturbulent velocities as a function of effective temperature. The CP stars from Paper I are shown as open stars, whereas the non-CP stars are indicated as open circles. The CP and non-CP objects from this work are presented as filled stars and circles, respectively. Diamonds show results from Kahraman Aliçavuş et al. (2016).

The relation between ξ_t and $\log g$ was also checked. This dependence was analysed by Gray et al. (2001) for the broad range of $\log g$ from 1.0 to 5.0. They discovered the clear correlations between $\log g$ and ξ_t for spectral types from A5 to G2. The microturbulent velocity in giants and supergiants is generally larger than in dwarfs. Our targets occupy a narrow $\log g$ range on or near the main sequence, preventing verification of the Gray et al. (2001) result.

As in Paper I, the determined microturbulent velocities of Am stars are similar to those of non-CP stars. The distribution of microturbulent velocities among the Am stars is indistinguishable from that of normal stars. This is in stark contrast to results presented by Landstreet et al. (2009), who claimed that Am stars have higher

microturbulent velocities, amid criticism of inadequate sampling (Murphy 2014).

4.2 Projected rotation velocity

The stars analysed here have projected rotational velocities ranging from 4 to 270 km s^{-1}. In Fig. 6(a) the distribution of the $v\sin i$ values obtained here and in Paper I is shown.

Stars with $v\sin i$ lower than 30 km s^{-1} are considered here as slowly rotating stars. There are seven such objects in the sample analysed here, including KIC 3868420 (A9 Vs) showing weakness of Ca lines and KIC 8694723 (hF6 mF2 gF5 V) that shows metal underabundances. There are four single non-CP stars with low $v\sin i$: KIC 7798339 (F1.5 V), KIC 9845907 (A4 IVs), KIC 9410862 (F6 V) and KIC 6370489 (F5.5 V). The slow rotation of F stars is also surprising, if the spectral type is earlier than F5, where the Kraft break is seen (Kraft 1967). Early F stars have a continuous rotational velocity distribution with late A stars. One of the stars, KIC 9408694 (F0 IVs+?) is a member of binary system.

Fig. 6(b) shows the distribution of $v\sin i$ for all non-CP stars analysed here and in Paper I. The mean value of $v\sin i$ for the whole sample is 125 km s^{-1} and the median is 110 km s^{-1}. These results are consistent with the projected rotational velocities of A stars available in the literature. Abt (2000) discovered that most of the non-CP A0–F0 main-sequence stars have $v\sin i$ values greater than 120 km s^{-1}. The average projected rotation velocity of about 130 km s^{-1} was determined by e.g. Royer (2009) and Abt (2009). Our results are consistent with their conclusions.

The occurrence of non-CP A stars with low $v\sin i$ has been discussed in Paper I. Various authors have tried to explain the origin of such stars. Abt (2009) considered binarity and the amount of time necessary for slow rotators to become Ap or Am stars by a diffusion mechanism (Talon, Richard & Michaud 2006; Michaud & Richer 2013). A more probable reason for the low observed $v\sin i$ in some A stars is the inclination effect, as for Vega (Gray 1985; Gulliver, Hill & Adelman 1994; Abt 2009; Hill, Gulliver & Adelman 2010). The spectroscopically obtained $v\sin i$ is a projection of the equatorial velocity along the line of sight, so stars classified as slow rotators can be in fact fast rotators seen at low inclination angle. To investigate the effect of low inclination on the observed spectrum of a fast rotator, high-resolution and very high S/N (∼1000) spectra are necessary (e.g. Royer et al. 2012).

5 CHEMICAL ABUNDANCES

In Table 3 the average abundances for a sample of non-CP and for all stars are compared with the photospheric solar values of Asplund et al. (2009). The abundances of C, Mg, Si, Ca, Sc, Ti, Cr and Fe were derived for all stars. For O we used lines that are only slightly affected by non-LTE effects (e.g. 5331, 6157, 6158, and 6456 Å; Przybilla et al. 2000). Lines of heavy elements except for Sr, Y, Zr, Ba and rare-earth elements are very sparse in spectra of A stars. Their abundances were investigated only for slowly and moderately rotating stars and in most cases only one or two blends were available.

5.1 Chemically peculiar stars

In Fig. 7, the determined average abundances for CP and non-CP stars are compared with the solar abundances of Asplund et al. (2009). The average abundances of most of the light and iron-peak elements are similar to the solar values. The largest differences were
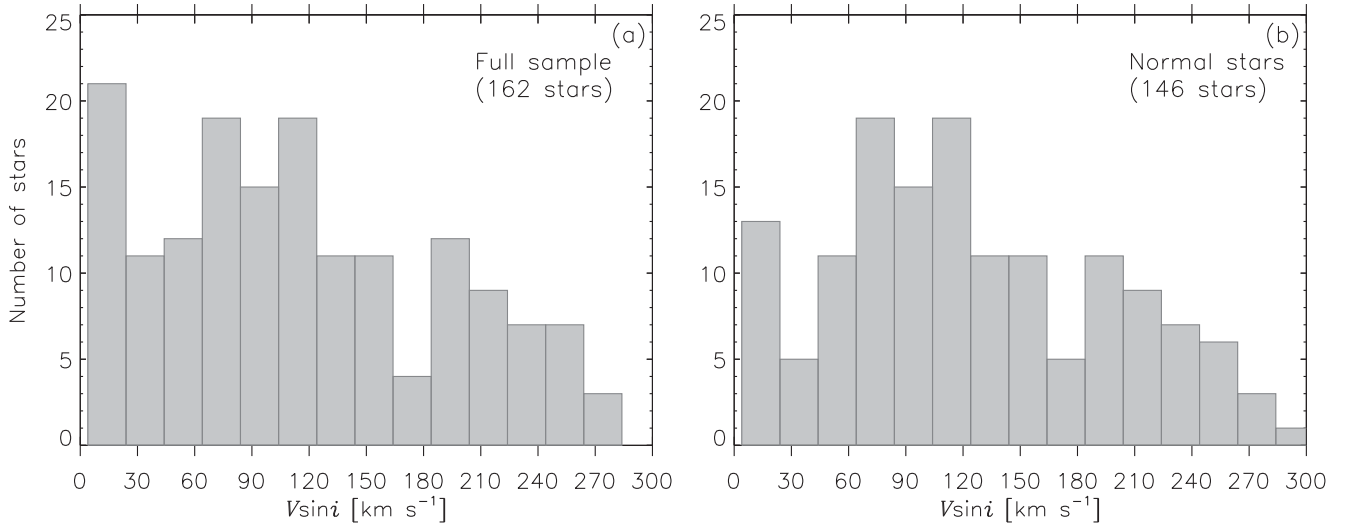
Figure 6. The distribution of rotational velocities for all stars (panel a) and for all non-CP stars (panel b) analysed here and in Paper I.

Table 3. Average abundances ($\log \epsilon$(El)), standard deviations and number of stars used for abundance calculations for non-CP, Am and λ Boo stars, compared to the reference solar values of Asplund et al. (2009).

El.	Non-CP stars	Am stars	λ Boo stars	Solar values
C	8.37, 0.25 (37)	8.26, 0.28 (4)	8.40, 0.08 (3)	8.43
N	8.17, 0.30 (7)	8.72 (1)	8.31 (1)	7.83
O	8.84, 0.25 (31)	8.68, 0.32 (4)	8.69, 0.20 (3)	8.69
Na	6.45, 0.43 (30)	6.59, 0.12 (4)	6.20 (1)	6.24
Mg	7.69, 0.24 (37)	7.71, 0.27 (4)	6.95, 0.51 (3)	7.60
Al	6.38, 0.36 (7)	6.73, 0.08 (2)		6.45
Si	7.50, 0.24 (37)	7.71, 0.05 (4)	6.96, 0.33 (3)	7.51
S	7.38, 0.27 (29)	7.39, 0.22 (4)	6.58 (1)	7.12
Ca	6.42, 0.26 (37)	6.09, 0.47 (4)	5.85, 0.37 (3)	6.34
Sc	3.17, 0.28 (37)	2.97, 0.29 (4)	2.58, 0.59 (3)	3.15
Ti	5.01, 0.21 (37)	5.16, 0.17 (4)	4.11, 0.26 (3)	4.95
V	4.33, 0.40 (28)	4.80, 0.15 (4)	4.07 (1)	3.93
Cr	5.62, 0.22 (37)	6.09, 0.10 (4)	4.79, 0.19 (3)	5.64
Mn	5.36, 0.29 (37)	5.41, 0.25 (4)	4.65 (1)	5.43
Fe	7.40, 0.24 (37)	7.76, 0.13 (4)	6.57, 0.24 (3)	7.50
Co	5.43, 0.64 (16)	5.49, 0.13 (2)	4.73 (1)	4.99
Ni	6.24, 0.31 (37)	6.68, 0.20 (4)	5.77, 0.13 (2)	6.22
Cu	4.15, 0.44 (23)	4.63, 0.26 (3)	4.13 (1)	4.19
Zn	4.41, 0.31 (26)	4.86, 0.31 (4)	3.98 (1)	4.56
Ga	2.94, 0.69 (4)	3.70, 0.45 (2)		3.04
Sr	2.99, 0.85 (36)	3.98, 0.09 (4)	2.49, 0.66 (2)	2.87
Y	2.37, 0.38 (33)	2.99, 0.05 (4)	1.84, 0.18 (2)	2.21
Zr	3.03, 0.34 (29)	3.09, 0.14 (4)	2.58 (1)	2.58
Ba	2.78, 0.53 (36)	3.82, 0.14 (4)	1.51, 0.25 (3)	2.18
La	1.43, 0.44 (22)	2.39, 0.19 (3)	1.16 (1)	1.10
Ce	1.97, 0.34 (15)	2.76, 0.11 (3)	1.47 (1)	1.58
Pr	0.73, 0.39 (6)	1.67 (1)		0.72
Nd	1.86, 0.47 (18)	2.48, 0.11 (3)	1.75 (1)	1.42
Sm	1.28, 0.54 (5)			0.96
Eu	1.28, 0.95 (5)	2.01 (1)		0.52
Gd	1.27, 0.34 (4)			1.07
Dy	1.11, 0.50 (4)			1.10
Er	1.49, 0.14 (3)			0.92

derived for the elements represented by weak blends only. As expected, the abundances of some elements determined for CP stars are far different from the solar values. The CP stars in our sample consist of regular and mild Am stars and λ Boötis candidates.

According to the abundance analysis, five stars were classified as Am:, three single stars KIC 3868420, KIC 7767565 and KIC 9941662, EB system KIC 2162283 and SB2 star KIC 3858884, the primary of which is a mild Am star (kA8 hF0 mF2.5 III). A detailed abundance analysis of SB2 systems, including KIC 3858884, will be presented in a forthcoming paper (Catanzaro et al., in preparation), because disentangling the spectral components from each star demands a different methodology.

KIC 3868420 was classified initially as A9 Vs with a very weak Ca II K line in comparison with the hydrogen line type. However, no metal line enhancement was detected under spectral classification. From the abundance analysis KIC 3868420 is a typical Am star with underabundant Ca and Sc but enhanced metal lines. KIC 7767565 (kA5 hA7 mF1 IV) shows the typical Am abundance pattern except for apparently normal Ca and Sc abundances. The star was classified as an Am in Paper I and the same spectral type was found here. For KIC 9941662 (kA2 hA5m A7 (IV)) the spectroscopic data analysis revealed lower Ca and Sc abundances, typical for Am stars.

KIC 2162283 was classified as a star with a composite Am + F spectrum. The spectral type obtained from hydrogen line is roughly consistent with an A9 giant. On the other hand, the extremely strong metal lines match a mid- or late-F star. The star shows overabundances of most iron-peak elements and some heavy elements like Zn, Sr, Zr and Ba, typical for an Am type, but the expected underabundance of Sc is small and Ca has normal abundance, contrary to expectation (Gray & Corbally 2009). From spectral classification the spectrum could be interpreted as an Am or Ap star due to the selective enhancements. The fact that Ca is not weak might appear to rule out an Am type, but the overall metal line morphology is best described by a composite spectrum, in which case the Ca II K line would be the mix of a weak Am type and a strong late-F type, and thus appear normal. Further, the strength of the overall metal line spectrum (in addition to the selective enhancement of some elements) is not typical of Ap stars, and this star is a known eclipsing binary.

KIC 3429637 (hA8 kF0 mF0 IIIas) was previously classified as hA9 kF2 mF3 type by Abt (1984) and as F0 III star by Catanzaro et al. (2011). KIC 3429637 is not an Am star. It's a giant with slightly enhanced metal lines.

There are three candidate λ Boötis stars in our sample: KIC 9656348, KIC 9828226 and KIC 11973705. They are
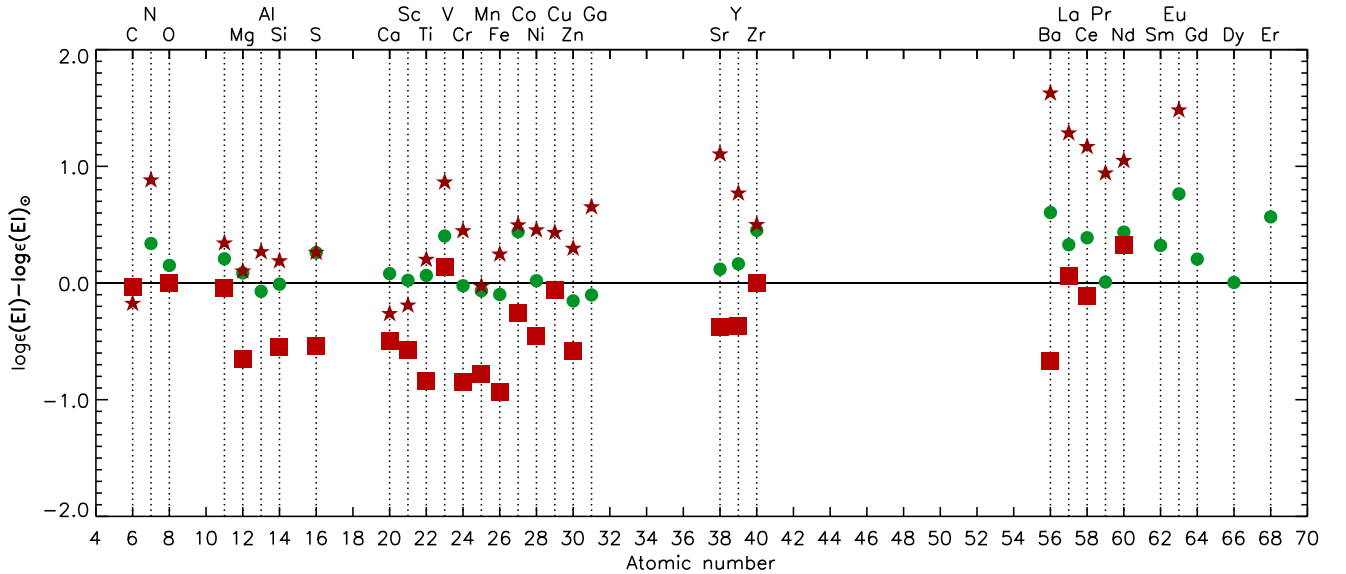
Figure 7. Average abundances of the non-CP (circles), Am (stars) and λ Boötis stars (squares) compared to the solar values of Asplund et al. (2009).

characterized by a weak Mg II 4481 line and solar abundances of C, N, O and S (Gray & Corbally 2009). The spectrum of KIC 9656348 (hA9 kA4 mA4 V) has hydrogen lines with deep cores but the core–wing boundaries and the wings themselves are narrow. Metal lines are also narrow and fit between A3 and A5 V, hence rotation cannot explain the metal weakness. KIC 9828226 (hA2 kB9.5 mB9 Vb) has tremendously broad hydrogen lines in the spectrum, hence the Vb luminosity class. Its Mg II 4481 line is weaker than the metal line type, that is, even weaker than at B9. Other metals are barely discernible. Hence, KIC 9828226 is a firm λ Boo candidate. This star was analysed in Paper I, where similar spectral type (hA2 kA0 mB9 Vb) and atmospheric parameters were found. Its moderate rotational velocity, 99 ± 18 km s^{-1}, allowed us to obtain the abundances of C, O, Mg, Si, Ca, Sc, Ti, Cr, Fe and Ba. The chemical abundances were determined on the basis of one or two lines only, except for Ti, Cr and Fe. All these elements are underabundant. The C and O abundances are solar, typical for λ Boötis stars. KIC 11973705 (hF0.5 kA2.5 mA2.5 V) has a typical λ Boo spectrum, with pronounced metal weakness and broad-but-shallow hydrogen line wings. Its abundances support the λ Boo classification.

In addition, a metal-weak late-type star was found. KIC 8694723 was classified as hF6 mF2 gF5 V, with hydrogen lines matching an F6 star, but noticeably weaker metal lines and *G* band.

5.2 Correlation of chemical abundances with other parameters

We used the stars analysed here and those from Paper I to search for possible correlations between the abundances of chemical elements and other stellar parameters. Also in this case we used the Kendall's rank correlation coefficient. Any correlations or anticorrelations found between abundances and atmospheric parameters are very useful for investigating hydrodynamical processes in stellar atmospheres. Because of the large sample of stars, we are able to make the reliable analysis of possible correlations between chemical abundances and $T_{\rm eff}$, log g, $\xi_{\rm t}$, $v$sin i and Fe abundances. Only in a few cases was the analysis complicated by large scatter or by having only a small number of stars with measured abundances

of a particular element. This is the case for some of the heavy and rare-earth elements.

Usually, chemically normal stars showed most mild correlation between element abundances and atmospheric parameters. Strong positive correlations with $T_{\rm eff}$ were only calculated for Zn (0.43) and Ce (0.57). In the case of Zn, the positive correlation can be eliminated by removing the low-temperature outliers. Any other correlations can be explained by small number of abundance calculations for a given element, rendering the correlation determination uncertain. Similarly, at mild correlations with log g and $\xi_{\rm t}$ were found. As expected, positive correlations with iron abundance were found for almost all elements. The highest correlation coefficients were obtained for iron-peak elements Ca, Ti, Cr, Ni, Cu, plus Al, La and Ce, all of which have correlation coefficients >0.30. Takeda et al. (2008) also found strong positive correlations between the abundances of Si, Ti and Ba, and that of Fe.

For CP stars, mild positive correlations (obtained for Al, S, Mn, Ni, Cu, Zn, Sr, Zr, Ba and La) may again be the result of small number statistics but this time because CP stars are few in number. Richer, Michaud & Turcotte (2000) also predicted mild correlations between abundances of some elements (e.g. Ni) and $T_{\rm eff}$. Strong correlations with $T_{\rm eff}$ were found only for Ca (0.52), O, Co and Ce (~ -0.40). Strong positive correlations with log g were found for Na, V, Mn, Cu and Zn (0.30–0.50). The strongest positive correlation was found for Ni (0.62), while negative were obtained for N (-0.62) and Sc (-0.33). The strong positive correlations with $\xi_{\rm t}$ were found for N (0.55), Cr (0.32) and Mn (0.39), while negative correlations were derived for C (-0.38) and Ba (-0.41). However, values for the smallest $\xi_{\rm t}$ sometimes differ significantly from the other results. Removing these values erases any existing correlations. Positive correlations (>0.30) with iron abundances were obtained for Na, Si, Ca, Ti, V, Cr, Mn, Ni and La. All correlations for CP should be treated with caution, because of the small number of the analysed CP stars.

In the present work, no strong correlations between the abundances of most elements and $v$sin i were found among normal stars. Stronger correlations were found only for Co (0.54), Nd (0.41) and Sr (-0.40). Only for Co and Sr can the correlation be considered as reliable, since for the other elements the number of stars considered
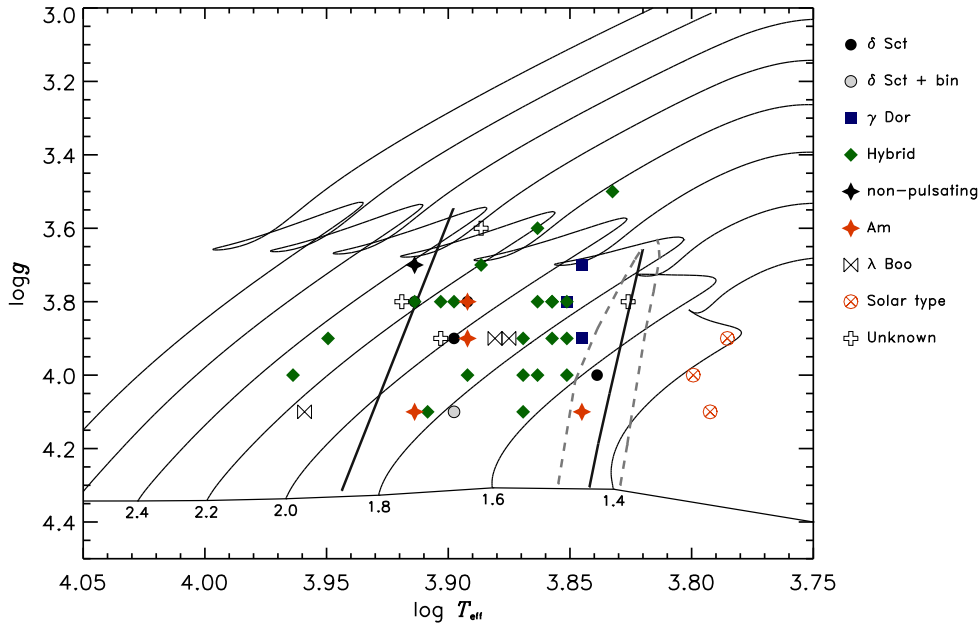
Figure 8. log T_{eff}–log g diagram for stars analysed in the current work. Stars identified as δ Sct, γ Dor, hybrids, non-pulsating or CP objects are plotted with different symbols (see legend).

is less than 20. For CP stars strong positive correlations were found for Na, Si, Ti, Mn and Co, with correlation coefficients higher than 0.40. Comparing samples with A and F stars, we found a larger scatter of abundances for hotter stars, especially for stars with $v\sin i$ higher than 150 km s^{-1}.

The same trend was obtained for the abundances of A and F stars in the Hyades (Gebran et al. 2010), Pleiades (Gebran & Monier 2008) and Coma Berenices open clusters (Gebran, Monier & Richard 2008). The correlations between abundances and $v\sin i$ were examined by Fossati et al. (2008) and Takeda et al. (2008). Fossati et al. (2008) investigated 23 normal A and F stars and found no correlation between abundances and projected rotational velocity. A larger sample was studied by Takeda et al. (2008), who discovered negative correlations for C, O, Ca and strong positive correlations for the Fe-peak elements plus Y and Ba, with rotational velocity.

6 VARIABILITY AND SPECTROSCOPIC H–R DIAGRAM

The atmospheric parameters obtained in this work are necessary ingredients for seismic modelling. Our sample of A and F stars contains pulsating δ Sct, γ Dor and hybrid stars. To find out if the atmospheric parameters of the analysed stars are consistent with theoretical instability strips in this part of the H–R diagram, we performed an analysis of the *Kepler* data for all objects investigated here. We used the multiscale MAP light curves available through the MAST[4] data base. We considered all the long cadence data available for a given star. If necessary, short cadence data were used to verify our classification. We visually examined all light curves, the frequency spectra and detected frequencies to identify candidate δ Sct, γ Dor, hybrid and other types of variability. The results of our initial classification are presented in the last column of Table 1.

Most of the stars were classified as hybrid δ Sct/γ Dor variables (29), including two stars showing HADS pulsations with possible γ Dor frequencies (KIC 3868420 and KIC 9408694). In this work, all objects for which we can find frequencies typical for δ Sct and γ Dor stars are termed 'hybrid'. We classified eight stars as δ Sct (single stars and binary systems), and four as pure γ Dor variables. For four stars the classification was not clear, so we denoted these stars as 'unknown' variables. Three of these stars have early spectral types from A3 to A6, all with luminosity class V (KIC 5880360, KIC 8211500 and KIC 11622328) but they show variability with frequencies typical for γ Dor stars. The other 'unknown' is the F6 III star, KIC 10341072. Two stars were classified as constant: KIC 9349245 and KIC 9941662. The latter has planetary transits (Kepler-13; Shporer et al. 2014). Solar-like oscillations were discovered for the three stars with the lowest temperature: KIC 9410862, KIC 8694723 (metal weak star hF6 mF2 gF5 V) and KIC 6370489. Moreover, we found six pulsating stars in binary systems, including eclipsing binaries (KIC 2162283, KIC 3858884 and KIC 10661783).

All of the investigated stars are shown in the T_{eff}–log g diagram (Fig. 8). Evolutionary tracks, calculated with time-dependent convection (TDC; Grigahcène et al. 2005), for stars having [Fe/H] =0.0 and $\alpha_{MLT} = 1.8$, covering a range of masses from 1.4 to 2.8 M$_\odot$ are plotted. The instability strips for δ Sct (solid line) and γ Dor (dashed line) are shown as well. As can be seen in Fig. 8, all the Am stars are located firmly inside the instability strip. Only one Am star was classified as a non-pulsating star (KIC 9941662), two are δ Sct stars (KIC 2162283 and KIC 3858884) one is γ Dor (KIC 7767565), and one is possible hybrid (KIC 3868420). As for the λ Boo stars, one is located inside the δ Sct instability strip (KIC 11973705) and one is hotter (KIC 9828226). All λ Boo stars were classified as δ Sct/γ Dor variables. Two chemically normal stars are located well outside the blue edge of the δ Sct instability strip, KIC 11044547, classified as possible hybrid with clear δ Sct and possible γ Dor frequencies, and KIC 9650390 classified as a clear hybrid star. Their temperatures are too high for hybrid δ Sct/γ Dor stars.

These two stars need further investigation to verify the possibility of contamination by another star. The other hybrid stars are located inside the δ Sct instability strip.

7 CONCLUSIONS

We have analysed FIES/NOT spectra of 50 A and F stars observed by *Kepler*. Spectral classification showed that our sample consists mostly of non-evolved stars of luminosity types V to IV and revealed nine CP stars of Am and λ Boötis types. Six of them were discovered as new CP stars. Atmospheric peculiarities of these stars were confirmed by detailed investigation of their stellar spectra.

We determined atmospheric parameters – $T_{\rm eff}$, $\log g$, $\xi_{\rm t}$, $v\sin i$ and chemical abundances – using spectral synthesis. Initial values of $T_{\rm eff}$ and $\log g$ were derived from H2014 (mostly photometric values), SED and Balmer lines analysis. For discussion of the parameters we used an enlarged sample of stars, including those analysed in Paper I, using the same method. The combined sample consists of 167 stars. We have confirmed that atmospheric parameters obtained from photometry (e.g. H2014), particularly $\log g$, are markedly inferior to those obtained spectroscopically from iron lines. The ability of photometry to derive these quickly for a large number of stars means this method will continue to have a role in input catalogues for space telescopes, but spectroscopy should be utilized when high accuracy and precision are required.

We have mapped the change in microturbulent velocities as a function of $T_{\rm eff}$ for normal stars and for Am stars in a self-consistent manner, and buck the trend in finding no microturbulence excess for Am stars over normal stars. We confirm suspicions that earlier results of that nature (e.g. Landstreet et al. 2009) failed to account for the increase in microturbulence for *all* stars in the 7000–8000 K temperature range where Am stars are predominantly found (Murphy 2014). We also find no correlation between $\xi_{\rm t}$ and $v\sin i$. The narrow $\log g$ range among our targets prevented a similar analysis for that parameter.

The stars analysed here have $v\sin i$ values ranging from 4 to about 280 km s^{-1}. There are seven objects with $v\sin i < 30$ km s^{-1} in our sample, including CP and non-CP stars. The mean value of $v\sin i$ for the whole sample is 125 km s^{-1}, and the median is 110 km s^{-1}, consistent with literature results for A/F stars in general (e.g. Royer 2009). Abundances are hard to measure for rapidly rotating A stars, but we confirm that they show large star-to-star variations (Hill & Landstreet 1993), especially where $v\sin i$ exceeds 150 km s^{-1}.

Homogeneous analysis of large samples of A and F stars frames the discussion of the nature of their atmospheres, e.g. the $v\sin i$ distribution and the influence of fast rotation on chemical abundances, and the dependence of microturbulent velocity on effective temperature and surface gravity. This provides a platform for greater understanding of atomic diffusion, mixing processes and angular momentum transport, which are extremely important but remain ill-understood. In addition, the provision of reliable stellar atmospheric parameters from spectroscopy is crucial to successful asteroseismic investigation of these objects, extending analyses from the line-forming region analysed spectroscopically to the deep interior of A/F stars probed by g-modes (Kurtz et al. 2014; Saio et al. 2015; Murphy et al. 2016; Schmid & Aerts 2016).

In the next papers we enlarge our sample for the other A–F stars from the *Kepler* field (Polińska et al., in preparation) as well as *K2* fields (Niemczura et al., in preparation). Both samples consist of possible δ Sct, γ Dor and hybrid stars. All the stars will be analysed with the same methods, using the same atmospheric models, and atomic data. The enlarged sample will consist of about 300 stars, what let us to observationally define instability regions for A–F pulsating stars. In addition, we check the possible correlations of pulsational characteristics of stars, obtained from *Kepler* data analysis with their atmospheric parameters and projected rotational velocity.

REFERENCES

Abt H. A., 1984, ApJ, 285, 247
Abt H. A., 2000, ApJ, 544, 933
Abt H. A., 2009, AJ, 138, 28
Armstrong D. J., Gómez Maqueo Chew Y., Faedi F., Pollacco D., 2014, MNRAS, 437, 3473
Asplund M., Grevesse N., Sauval A. J., Scott P., 2009, ARA&A, 47, 481
Balona L. A., 2013, MNRAS, 431, 2240
Balona L. A., 2014, MNRAS, 441, 3543
Balona L. A., Dziembowski W., 2011, MNRAS, 417, 591
Balona L. A. et al., 2011, MNRAS, 413, 2403
Balona L. A. et al., 2012, MNRAS, 419, 3028
Balona L. A., Baran A. S., Daszyńska-Daszkiewicz J., De Cat P., 2015, MNRAS, 451, 1445
Brown T. M., Latham D. W., Everett M. E., Esquerdo G. A., 2011, AJ, 142, 112
Bruntt H. et al., 2012, MNRAS, 423, 122
Carnochan D. J., 1979, Bull. Inf. CDS, 17, 78
Castelli F., Hubrig S., 2004, A&A, 425, 263
Catanzaro G, Leone F., Dall T. H., 2004, A&A, 425, 641
Catanzaro G. et al., 2011, MNRAS, 411, 1167
Catanzaro G. et al., 2015, MNRAS, 451, 184
Chaffee F. H., Jr, 1970, A&A, 4, 291
Chaplin W. J. et al., 2014, ApJS, 210, 1
Coupry M. F., Burkhart C., 1992, A&AS, 95, 41
Edvardsson B., Andersen J., Gustafsson B., Lambert D. L., Nissen P. E., Tomkin J., 1993, A&A, 275, 101
Fossati L., Bagnulo S., Landstreet J., Wade G., Kochukhov O., Monier R., Weiss W., Gebran M., 2008, A&A, 483, 891
Gebran M., Monier R., 2008, A&A, 483, 567
Gebran M., Monier R., Richard O., 2008, A&A, 479, 189
Gebran M., Vick M., Monier R., Fossati L., 2010, A&A, 523, A71
Gebran M., Monier R., Royer F., Lobel A., Blomme R., 2014, in Mathys G., Griffin E., Kochukhov O., Monier R., Wahlgren G., eds, Putting A Stars into Context: Evolution, Environment, and Related Stars. Publishing House 'Pero', Moscow, p. 193
Gilliland R. L., Chaplin W. J., Jenkins J. M., Ramsey L. W., Smith J. C., 2015, AJ, 150, 133
Gray R. O., 1985, J. R. Astron. Soc. Canada, 79, 237
Gray D. F., 2005, The Observation and Analysis of Stellar Photospheres, 3rd edn. Cambridge Univ. Press, Cambridge
Gray R. O., Corbally C. J., 2009, Stellar Spectral Classification. Princeton Univ. Press, Princeton, NJ
Gray R. O., Graham P. W., Hoyt S. R., 2001, AJ, 121, 2159
Grigahcène A., Dupret M.-A., Gabriel M., Garrido R., Scuflaire R., 2005, A&A, 434, 1055
Grigahcène A. et al., 2010, ApJ, 713, L192
Gulliver A. F., Hill G., Adelman S. J., 1994, ApJ, 429, L81
Guzik J. A., Bradley P. A., Jackiewicz J., Molenda-Zakowicz J., Uytterhoeven K., Kinemuchi K., 2015, Astron. Rev., in press (arXiv:1502.00175)

Heckmann O., Dieckvoss W., 1975, AGK3 Catalogue
Hill G., Landstreet J. D., 1993, A&A, 276, 142
Hill G., Gulliver A. F., Adelman S. J., 2010, ApJ, 712, 250
Howarth I. D., 1983, MNRAS, 203, 301
Howell S. B. et al., 2014, PASP, 126, 398
Huber D. et al., 2014, ApJS, 211, 2 (H2014)
Kahraman Aliçavuş F. et al., 2016, MNRAS, 458, 2307
Karoff C. et al., 2013, MNRAS, 433, 3227
Kharchenko N. V., 2001, Kinematika i Fizika Nebesnykh Tel, 17, 409
Kjeldsen H., Christensen-Dalsgaard J., Handberg R., Brown T. M., Gilliland
    R. L., Borucki W. J., Koch D., 2010, Astron. Nachr., 331, 966
Kraft R. P., 1967, ApJ, 150, 551
Kurtz D. W, Saio H., Takata M., Shibahashi H., Murphy S. J., Sekii T., 2014,
    MNRAS, 444, 102
Kurucz R. L., 1993a, Kurucz CD-ROM 13. SAO, Cambridge, MA
Kurucz R. L., 1993b, Kurucz CD-ROM 18. SAO, Cambridge, MA
Kurucz R. L., 2011, Can. J. Phys., 89, 417
Lampens P. et al., 2013, A&A, 549, A104
Landstreet J. D., Kupka F., Ford H. A., Officer T., Sigut T. A. A., Silaj J.,
    Strasser S., Townshend A., 2009, A&A, 503, 973
Lehmann H. et al., 2011, A&A, 526, A124
Lehmann H., Southworth J., Tkachenko A., Pavlovski K., 2013, A&A, 557,
    A79
Lindoff U., 1972, A&A, 16, 315
McDonald I., Zijlstra A. A., Boyer M. L., 2012, MNRAS, 427, 343
Macrae D. A., 1952, ApJ, 116, 592
Mashonkina L., 2011, in Romanyuk I. I., Kudryavtsev D. O., eds, Magnetic
    Stars. EDP Sciences, Moscow, p. 314
Michaud G., Richer J., 2013, EAS Publ. Ser., 63, 199
Molenda-Żakowicz J. et al., 2013, MNRAS, 434, 1422
Mortier A., Sousa S. G., Adibekyan V. Z., Brandão I. M., Santos N. C.,
    2014, A&A, 572, A95
Munari U., Zwitter T., 1997, A&A, 318, 26
Murphy S. J., 2014, PhD thesis, Univ. Central Lancashire
Murphy S. J., Grigahcène A., Niemczura E., Kurtz D. W., Uytterhoeven K.,
    2012, MNRAS, 427, 1418
Murphy S. J., Bedding T. R., Niemczura E., Kurtz D. W., Smalley B., 2015,
    MNRAS, 447, 3948
Murphy S. J., Fossati L., Bedding T. R., Saio H., Kurtz D. W., Grassitelli L.,
    Wang E. S., 2016, MNRAS, 459, 1201
Nemec J. M., Cohen J. G., Ripepi V., Derekas A., Moskalik P., Sesar B.,
    Chadid M., Bruntt H., 2013, ApJ, 773, 181
Niemczura E. et al., 2015, MNRAS, 450, 2764 (Paper I)
Nordstrom B., Stefanik R. P., Latham D. W., Andersen J., 1997, A&AS,
    126, 21
Przybilla N., Butler K., Becker S. R., Kudritzki R. P., Venn K. A., 2000,
    A&A, 359, 1085
Renson P., Manfroid J., 2009, A&A, 498, 961
Richer J., Michaud G., Turcotte S., 2000, ApJ, 529, 338
Royer F., 2009, in Rozelot J.-P., Neiner C., eds, Lecture Notes in Physics,
    Vol. 765, The Rotation of Sun and Stars. Springer-Verlag, Berlin,
    p. 207
Royer F. et al., 2012, in Boissier S., de Laverny P., Nardetto N., Samadi R.,
    Valls-Gabaud D., Wozniak H., eds, Proceedings of the Annual meeting
    of the French Society of Astronomy and Astrophysics, Société Francaise
    d'Astronomie et d'Astrophysique (SF2A)-2012, p. 389
Ryabchikova T. et al., 2016, MNRAS, 456, 1221
Saio H., Kurtz D. W., Takata M., Shibahashi H., Murphy S. J., Sekii T.,
    Bedding T. R., 2015, MNRAS, 447, 3264
Sbordone L., 2005, Mem. Soc.à Astron. Ital. Suppl., 8, 61
Schmid V. S., Aerts C., 2016, A&A, 592, A116
Seaton M. J., 1979, MNRAS, 187, 73
Shporer A. et al., 2014, ApJ, 788, 92
Smalley B., 2004, in Zverko J., Ziznovsky J., Adelman S. J., Weiss W. W.,
    eds, Proc. IAU Symp. 224, The A-Star Puzzle. Cambridge Univ. Press,
    Cambridge, p. 131
Smalley B. et al., 2015, MNRAS, 452, 3334
Southworth J. et al., 2011, MNRAS, 414, 2413

Takeda Y., Han I., Kang D. I., Lee B. C., Kim K. M., 2008, J. Korean Astron.
    Soc., 41, 83
Talon S., Richard O., Michaud G., 2006, ApJ, 645, 634
Telting J. H. et al., 2014, Astron. Nachr., 335, 41
Tkachenko A., Lehmann H., Smalley B., Debosscher J., Aerts C., 2012,
    MNRAS, 422, 2960
Tkachenko A. et al., 2013a, A&A, 556, A52
Tkachenko A., Lehmann H., Smalley B., Uytterhoeven K., 2013b, MNRAS,
    431, 3685
Ulusoy C. et al., 2013, MNRAS, 428, 3551
Uytterhoeven K. et al., 2010, Astron. Nachr., 331, 993
Uytterhoeven K. et al., 2011, A&A, 534, A125

SUPPORTING INFORMATION

Supplementary data are available at *MNRAS* online.

Please note: Oxford University Press is not responsible for the content or functionality of any supporting materials supplied by the authors. Any queries (other than missing material) should be directed to the corresponding author for the article.

APPENDIX A: COMPARISON WITH THE LITERATURE

Most stars presented in this work are analysed here for the first time. We summarize the literature on the remainder in this appendix.

(i) KIC 2162283 – eclipsing binary system. The star was analysed here as a single object and the results of all methods are consistent. Armstrong et al. (2014) combined the data from the photometric surveys to construct SED for this binary system and obtained primary and secondary stellar temperatures of 7530 ± 350 and 7520 ± 540 K.

(ii) KIC 3219256 – our results are consistent with each other. Catanzaro et al. (2011) used low-resolution data to obtain similar effective temperature 7500 ± 150 K and surface gravity 3.6 ± 0.1 dex.

(iii) KIC 3429637 – the atmospheric parameters obtained in this work are consistent. The effective temperatures from SED with TD1 (7340 K) and without TD1 data (7260 K) are also similar. Renson & Manfroid (2009) mentioned this star in the catalogue of CP objects, without pointing the peculiarity type. Catanzaro et al. (2011) analysed medium-resolution spectra and obtained effective temperature 7100 ± 150 K, similar to our value. The surface gravity determined by them, 3.00 ± 0.20 dex is lower that our value, 3.40 ± 0.10 dex. McDonald, Zijlstra & Boyer (2012) determined fundamental atmospheric parameters from the analysis of the high-resolution spectra. The atmospheric parameters obtained by them, effective temperature 7300 ± 100 K, surface gravity 3.0 ± 0.1 dex, microturbulence 4.0 ± 0.5 km s^{-1} and projected rotational velocity 51 ± 1 km s^{-1} are close to our results. They also confirmed earlier characterizations of KIC 3429637 as a marginal Am star.

(iv) KIC 3453494 – our results are consistent. The star was analysed by Tkachenko et al. (2012). They found similar effective temperature from SED analysis, 7840 ± 240 K, and from spectral analysis, 7737 ± 57 K. Also their log *g* value is consistent with our result. On the other hand, the microturbulence value obtained here, 2.00 ± 0.5 km s^{-1} is lower than 3.24 ± 0.66 km s^{-1}, determined by Tkachenko et al. (2012). It is the result of very fast rotation of this star, which makes it difficult to derive the correct value of microturbulence.

(v) KIC 3868420 – this star belongs to a multiple system consisting of two brighter and closer components, 10.35 and 10.61 mag,

with separation 2.5 arcsec, plus a wide (26 arcsec) third component with $V = 11.71$ mag. For this reason the photometric magnitudes used for SED construction are unreliable, as they were obtained for the combined light of the close pair. There is insufficient photometry of the individual stars to obtain SED fits for each star. Moreover, this is a HADS pulsator, so photometry will sample the star at different phases and brightnesses. Our results from Balmer and iron lines analysis are consistent. Nemec et al. (2013) defined this star as HADS with T_{eff} =7612 K, $\log g$ =3.71, ξ_t =2.3 km s^{-1}, macroturbulence 23.0 km s^{-1}and $v\sin i$ =5.7 km s^{-1} from spectrum synthesis. Their atmospheric parameters are consistent with our results except for microturbulence, which is lower. The differences in $v\sin i$ are caused by the inclusion of macroturbulence.

(vi) KIC 5988140 – results obtained here are consistent with each other and with Paper I. Catanzaro et al. (2011) found a lower T_{eff}, 7400 $\pm$ 150 K, but the same $\log g$, 3.7 $\pm$ 0.3, from the analysis of low-resolution spectroscopy. Lampens et al. (2013) found effective temperature 7600 $\pm$ 30 K, surface gravity 3.40 $\pm$ 0.12 dex, projected rotation velocity 52 $\pm$ 1.5 km s^{-1}and microturbulence 3.16 $\pm$ 0.20 km s^{-1} from high-resolution spectroscopy and spectrum synthesis.

(vii) KIC 5880360 – the atmospheric parameters obtained in this work are consistent. McDonald et al. (2012) determined effective temperature 7510 K from the SED analysis, significantly lower than the result obtained by us (8070 $\pm$ 220 K).

(viii) KIC 6370489 – our results are consistent. Molenda-Żakowicz et al. (2013) determined similar effective temperature 6241 $\pm$ 116 K and surface gravity 3.98 $\pm$ 0.21 dex from the analysis of high-resolution spectra. Also Chaplin et al. (2014) obtained similar effective temperatures of 6300 $\pm$ 80 and 6324 $\pm$ 144 K from photometric data.

(ix) KIC 7119530 – the results from iron lines analysis are consistent with Paper I. Catanzaro et al. (2011) determined a lower effective temperature, 7500 K, from low-resolution spectroscopy and Balmer-line analysis. Their surface gravity, 3.6 $\pm$ 0.3 dex, is consistent with ours.

(x) KIC 7748238 – the atmospheric parameters obtained in this work agree very well with each other. Tkachenko et al. (2012) found similar values of T_{eff} (7264 K), $\log g$ (3.96) and ξ_t (3.53 km s^{-1}) from high-resolution spectrum synthesis.

(xi) KIC 7798339 – our results are consistent. Nordstrom et al. (1997) analysed echelle spectra in the narrow wavelength range 5165.77–5211.25 Å to obtain $T_{eff} = 7000$ K, $\log g = 3.5$ and $v\sin i = 15.4$ km s^{-1}. These values are in good agreement with ours. Catanzaro et al. (2011) analysed medium-resolution spectra and obtained effective temperature 6700 $\pm$ 150 K and surface gravity 3.7 $\pm$ 0.3 dex, close to our results. McDonald et al. (2012) determined $T_{eff} = 6900$ K from SED analysis, consistent with ours.

(xii) KIC 8211500 – the atmospheric parameters obtained in this work are consistent. It is a binary system WDS 18462+4408 of stars with magnitudes 8.19 and 11.28 and separation 0.7 arcsec. The SED result is for combined light, but the large magnitude difference means that the faint companion should not affect the results. McDonald et al. (2012) determined $T_{eff} = 7709$ K in accordance with our results. Similarly, Murphy et al. (2015) gave $T_{eff} = 7800$ K and $\log g = 3.8$.

(xiii) KIC 8694723 – our results are consistent. Atmospheric parameters of this star determined from the analysis of high-resolution spectra were available before. Molenda-Żakowicz et al. (2013) obtained T_{eff} and $\log g$ (6287 $\pm$ 116 K, 4.00 $\pm$ 0.21), iron abundance (−0.38 $\pm$ 0.22) and $v\sin i$ value (3.8 $\pm$ 0.7 km s^{-1}) consistent with our results. Karoff et al. (2013) derived $T_{eff} = 6287 \pm 60$ K, $\log g = 4,079 \pm 0.035$, iron abundance -0.59 ± 0.06 and projected rotational velocity 6.6 km s^{-1} in accordance with our values. The atmospheric parameters and projected rotational velocities close to the values obtained here were also given by Bruntt et al. (2012). Higher effective temperatures (about 6400–6500 K) were determined by Mortier et al. (2014) from the equivalent width method and high-resolution spectroscopy.

(xiv) KIC 9349245 – the atmospheric parameter indicators adopted in this work agree very well with each other. Renson & Manfroid (2009) included this star in their catalogue of Ap, HgMn and Am stars, but without the classification of the peculiarity type. Balona (2013) classified this star as rotationally variable star on the basis of *Kepler* data. Balona (2014) determined the effective temperature of the star as 7690 K, lower than our results. Catanzaro et al. (2015) analysed the SED and high-resolution spectra and determined the atmospheric parameters of this star. The results from the SED (8250 $\pm$ 250 K) and from spectrum synthesis ($T_{eff} = 8300 \pm 200$ K, $\log g = 4.00 \pm 0.30$, $\xi_t = 3.1 \pm 0.5$ km s^{-1}and $v\sin i$ 80 $\pm$ 3 km s^{-1}) are consistent with the results of our analysis.

(xv) KIC 9408694 (V2367 Cyg) – is a HADS pulsator, so photometry used for SED construction can sample the star at different phases and brightnesses. Our results are consistent with each other, and in agreement with the values determined before. Balona et al. (2012) analysed low-resolution spectra and obtained T_{eff} 7300 $\pm$ 150 K, $\log g$ 3.5 $\pm$ 0.1 consistent with our results. Also Ulusoy et al. (2013) analysed low-resolution data to obtain similar values. The best fit to the Hβ and Hα lines was obtained for effective temperature 7250 K and surface gravity 3.5 dex.

(xvi) KIC 9410862 – our results are consistent. Chaplin et al. (2014) determined effective temperatures from SDSS (6230 $\pm$ 53 K) and IRFM (6143 $\pm$ 148 K) photometry, in agreement with our results.

(xvii) KIC 10030943 – this is an eclipsing binary. The atmospheric parameter indicators adopted in this work agree with each other, except for the SED T_{eff}. This may be the result of the influence of the secondary star on the photometric indices. Using photometric methods, Armstrong et al. (2014) determined atmospheric parameters of both objects, effective temperatures 6761 $\pm$ 354 and 6727 $\pm$ 549 K, respectively.

(xviii) KIC 10661783 – our results are consistent. This is an eclipsing binary of β Lyr type (semidetached). It was analysed by Southworth et al. (2011) as an eclipsing binary system with δ Sct pulsations. They determined temperatures of both stars at 8000 $\pm$ 160 and 6500 K. Lehmann et al. (2013) analysed physical properties of both stars and found effective temperatures (7764 $\pm$ 54, 5980 $\pm$ 72 K), surface gravities (3.9, 3.6 dex) and projected rotational velocities (79 $\pm$ 4, 48 $\pm$ 3 km s^{-1}). Our results are consistent with the atmospheric parameters of the primary component. In a catalogue of *Kepler* eclipsing binary stars, Armstrong et al. (2014) give wildly discordant effective temperatures of 9197 $\pm$ 475 and 7714 $\pm$ 808 K for primary and secondary, respectively.

(xix) KIC 11973705 – is a binary star, probably consisting of a late-B and a late-A star. We noted ellipsoidal variability in the *Kepler* light curve. The atmospheric parameters obtained in this work are consistent with each other, and correspond to the A star. The effective temperature from H2014 differs significantly from the other results, at 11 000 K.

Lehmann et al. (2011) performed spectral analysis of *Kepler* SPB and β Cep candidate stars. They classified this star as SPB with spectral type B8.5 V-IV (HD 234999) and determined $T_{\rm eff}$ from SED analysis (7920 $\pm$ 100 K) taking into account TD-1 data. The effective temperature obtained by Lehmann et al. (2011) from spectral analysis is similar to the one in H2014, 11 150 K. They therefore appear to have sampled both stars.

Catanzaro et al. (2011) noted that the spectral type recorded in the Henry Draper catalogue (B9), is an entire spectral class too early in comparison with their classification of A9.5 V. They classified the star as a δ Sct variable in a binary system. Their atmospheric parameters obtained from the analysis of low-resolution (R 5000) spectroscopy and 2MASS, uvbyβ and IRFM photometry are in accordance with our results.

Balona et al. (2011) searched *Kepler* observations for variability seen in B stars. The star was classified as the binary system with an SPB and a δ Sct component, with spectral type B8.5 V-IVb. In a catalogue of effective temperatures for *Kepler* eclipsing binary stars, Armstrong et al. (2014) gave 7918 $\pm$ 356 and 6528 $\pm$ 556 K, not particularly capturing the nature of either star. Balona et al. (2015) classified this star as Maia variable.

APPENDIX B: ADDITIONAL TABLES

Table B1. Abundances of chemical elements for the analysed stars (on the scale in which log ϵ(H) = 12). The median value is given; standard deviations were calculated only if the number of analysed parts or lines (depending on v sin i of the star) is greater than three. In other cases the average value calculated from standard deviations of other elements analysed for a given star are shown. Number of analysed parts or lines is given in brackets.

	KIC 10030943	KIC 10341072	KIC 10661783	KIC 10717871	KIC 11044547	KIC 11622328	KIC 11973705	KIC 2162283	KIC 2694337	KIC 3219256
C	8.65 ± 0.05 (6)	8.75 ± 0.10 (5)	8.17 ± 0.20 (4)	8.41 ± 0.25 (5)	8.49 ± 0.35 (5)	8.43 ± 0.14 (3)	8.45 ± 0.19 (2)	8.64 ± 0.37 (14)	8.58 ± 0.19 (10)	8.32 ± 0.11 (2)
N	–	–	8.42 ± 0.20 (1)	–	8.28 ± 0.18 (1)	–	–	8.72 ± 0.19 (2)	8.34 ± 0.17 (1)	–
O	8.93 ± 0.15 (1)	–	8.92 ± 0.20 (2)	9.02 ± 0.19 (1)	8.92 ± 0.18 (2)	8.93 ± 0.13 (2)	8.49 ± 0.19 (2)	9.17 ± 0.19 (2)	9.02 ± 0.17 (1)	8.78 ± 0.11 (1)
Ne	–	–	–	–	–	–	–	–	–	–
Na	5.98 ± 0.14 (3)	7.06 ± 0.09 (3)	6.58 ± 0.20 (2)	6.44 ± 0.19 (2)	6.80 ± 0.18 (1)	–	–	6.61 ± 0.13 (3)	6.70 ± 0.17 (2)	6.59 ± 0.11 (1)
Mg	7.30 ± 0.23 (6)	7.74 ± 0.23 (7)	7.79 ± 0.18 (5)	7.65 ± 0.12 (5)	7.68 ± 0.14 (8)	7.71 ± 0.05 (4)	–	7.63 ± 0.17 (8)	7.80 ± 0.12 (12)	7.66 ± 0.13 (4)
Al	–	6.73 ± 0.18 (1)	–	–	6.30 ± 0.18 (1)	–	6.81 ± 0.11 (3)	6.78 ± 0.19 (1)	–	–
Si	7.19 ± 0.24 (12)	7.69 ± 0.20 (13)	7.51 ± 0.32 (11)	7.52 ± 0.14 (10)	7.74 ± 0.15 (8)	7.61 ± 0.39 (3)	7.25 ± 0.37 (3)	7.65 ± 0.25 (36)	7.55 ± 0.20 (17)	7.82 ± 0.17 (7)
P	–	–	–	–	–	–	–	–	–	–
S	7.55 ± 0.15 (2)	7.75 ± 0.18 (2)	7.70 ± 0.20 (2)	7.14 ± 0.19 (2)	–	–	–	7.61 ± 0.16 (11)	7.39 ± 0.23 (3)	7.05 ± 0.11 (1)
Cl	–	–	–	–	–	–	–	–	–	–
K	–	–	–	–	–	–	–	–	–	–
Ca	6.18 ± 0.17 (15)	6.80 ± 0.25 (18)	6.33 ± 0.25 (13)	6.70 ± 0.22 (12)	6.78 ± 0.16 (15)	6.33 ± 0.10 (5)	5.48 ± 0.18 (8)	6.48 ± 0.21 (22)	6.68 ± 0.15 (13)	6.43 ± 0.11 (9)
Sc	2.94 ± 0.12 (5)	3.64 ± 0.15 (9)	3.36 ± 0.19 (6)	3.50 ± 0.39 (5)	3.37 ± 0.24 (6)	3.26 ± 0.04 (4)	2.11 ± 0.25 (3)	3.04 ± 0.23 (9)	3.21 ± 0.14 (9)	3.13 ± 0.08 (5)
Ti	4.92 ± 0.11 (25)	5.37 ± 0.22 (25)	5.18 ± 0.23 (21)	5.12 ± 0.26 (17)	5.20 ± 0.16 (27)	5.14 ± 0.09 (10)	4.03 ± 0.17 (10)	5.26 ± 0.20 (50)	5.13 ± 0.18 (23)	5.07 ± 0.14 (15)
V	4.23 ± 0.21 (3)	4.39 ± 0.35 (4)	4.10 ± 0.18 (4)	4.55 ± 0.19 (2)	4.87 ± 0.18 (2)	4.22 ± 0.13 (1)	–	4.89 ± 0.25 (9)	3.96 ± 0.27 (3)	–
Cr	5.42 ± 0.16 (20)	5.83 ± 0.21 (23)	5.80 ± 0.18 (18)	5.59 ± 0.20 (16)	5.70 ± 0.11 (16)	5.67 ± 0.12 (10)	4.66 ± 0.17 (5)	6.08 ± 0.19 (64)	5.71 ± 0.17 (23)	5.57 ± 0.12 (12)
Mn	5.30 ± 0.24 (4)	5.80 ± 0.25 (6)	5.15 ± 0.29 (6)	5.80 ± 0.09 (3)	5.48 ± 0.18 (2)	5.29 ± 0.13 (1)	–	5.47 ± 0.25 (17)	5.34 ± 0.13 (5)	5.07 ± 0.11 (2)
Fe	7.07 ± 0.10 (58)	7.63 ± 0.08 (45)	7.51 ± 0.12 (47)	7.45 ± 0.11 (45)	7.63 ± 0.13 (63)	7.40 ± 0.09 (27)	6.50 ± 0.14 (24)	7.71 ± 0.14 (187)	7.60 ± 0.07 (59)	7.40 ± 0.10 (45)
Co	–	5.96 ± 0.18 (2)	–	5.78 ± 0.19 (1)	–	–	–	5.59 ± 0.31 (4)	5.06 ± 0.17 (1)	–
Ni	5.95 ± 0.14 (21)	6.53 ± 0.21 (29)	6.22 ± 0.20 (13)	6.22 ± 0.14 (11)	6.61 ± 0.23 (8)	6.55 ± 0.22 (3)	5.67 ± 0.20 (5)	6.65 ± 0.18 (72)	6.36 ± 0.21 (25)	6.23 ± 0.10 (9)
Cu	4.45 ± 0.15 (2)	4.30 ± 0.09 (3)	3.36 ± 0.20 (1)	4.06 ± 0.19 (1)	–	–	–	4.54 ± 0.12 (3)	3.98 ± 0.17 (2)	–
Zn	4.39 ± 0.15 (1)	4.19 ± 0.18 (1)	–	4.21 ± 0.19 (1)	–	–	–	4.88 ± 0.19 (2)	3.96 ± 0.17 (1)	–
Ga	–	–	–	–	–	–	–	4.02 ± 0.19 (1)	–	–
Sr	3.08 ± 0.15 (1)	3.52 ± 0.18 (2)	3.43 ± 0.20 (1)	2.98 ± 0.19 (1)	3.11 ± 0.18 (1)	2.31 ± 0.13 (1)	2.02 ± 0.19 (1)	3.94 ± 0.01 (3)	3.39 ± 0.17 (2)	3.26 ± 0.11 (1)
Y	2.34 ± 0.18 (6)	2.76 ± 0.26 (5)	2.32 ± 0.12 (4)	2.47 ± 0.20 (3)	2.19 ± 0.18 (2)	1.82 ± 0.13 (1)	1.97 ± 0.19 (1)	3.02 ± 0.20 (15)	2.49 ± 0.21 (5)	–
Zr	2.87 ± 0.07 (4)	3.12 ± 0.01 (3)	2.78 ± 0.21 (3)	2.65 ± 0.23 (4)	3.90 ± 0.18 (1)	–	–	3.26 ± 0.26 (10)	3.05 ± 0.13 (5)	–
Ba	2.59 ± 0.13 (3)	2.90 ± 0.18 (2)	3.26 ± 0.20 (2)	2.80 ± 0.14 (3)	2.32 ± 0.18 (2)	2.77 ± 0.13 (1)	1.66 ± 0.19 (2)	3.64 ± 0.19 (4)	2.83 ± 0.17 (2)	3.05 ± 0.11 (2)
La	1.39 ± 0.15 (2)	1.35 ± 0.18 (1)	1.56 ± 0.20 (1)	1.61 ± 0.19 (1)	–	–	–	2.55 ± 0.10 (5)	1.73 ± 0.17 (1)	–
Ce	1.85 ± 0.15 (2)	–	–	–	–	–	–	2.85 ± 0.14 (12)	1.91 ± 0.17 (1)	–
Pr	–	–	–	–	–	–	–	–	–	–
Nd	2.08 ± 0.15 (2)	2.38 ± 0.18 (2)	–	–	–	–	–	2.43 ± 0.16 (9)	2.37 ± 0.17 (2)	–
Sm	–	–	–	–	–	–	–	–	–	–
Eu	–	2.49 ± 0.18 (1)	–	–	–	–	–	–	–	–
Gd	–	–	–	–	–	–	–	–	–	–
Dy	–	–	–	–	–	–	–	–	–	–
Er	–	–	–	–	–	–	–	–	–	–

Table B1 – *continued*

	KIC 3331147	KIC 3429637	KIC 3453494	KIC 3868420	KIC 4647763	KIC 5880360	KIC 5988140	KIC 6123324	KIC 6279848	KIC 6370489
C	8.36 ± 0.12 (12)	8.21 ± 0.14 (8)	7.97 ± 0.11 (2)	7.95 ± 0.30 (11)	8.31 ± 0.08 (5)	8.27 ± 0.16 (1)	8.33 ± 0.20 (7)	8.94 ± 0.18 (2)	8.08 ± 0.23 (13)	8.21 ± 0.22 (24)
N	–	–	–	–	–	–	–	–	–	–
O	9.15 ± 0.17 (1)	8.39 ± 0.13 (1)	8.43 ± 0.11 (1)	8.49 ± 0.16 (1)	–	–	8.72 ± 0.16 (1)	–	8.19 ± 0.17 (1)	8.52 ± 0.22 (1)
Ne	–	–	–	–	–	–	–	–	–	–
Na	6.52 ± 0.23 (3)	6.57 ± 0.13 (2)	–	6.67 ± 0.34 (6)	6.64 ± 0.26 (4)	–	5.32 ± 0.16 (1)	–	6.37 ± 0.23 (3)	5.95 ± 0.13 (10)
Mg	7.79 ± 0.04 (6)	7.77 ± 0.13 (5)	8.02 ± 0.01 (3)	7.42 ± 0.23 (13)	7.47 ± 0.10 (7)	7.23 ± 0.35 (4)	7.80 ± 0.05 (4)	7.43 ± 0.18 (2)	7.36 ± 0.18 (10)	7.37 ± 0.11 (12)
Al	–	–	–	6.67 ± 0.16 (1)	–	–	–	–	–	–
Si	7.60 ± 0.19 (25)	7.47 ± 0.17 (11)	7.98 ± 0.16 (4)	7.68 ± 0.25 (24)	7.48 ± 0.31 (12)	7.05 ± 0.16 (2)	7.62 ± 0.26 (11)	7.50 ± 0.18 (2)	7.36 ± 0.25 (19)	7.29 ± 0.26 (53)
P	–	–	–	–	–	–	–	–	–	–
S	7.28 ± 0.15 (4)	7.45 ± 0.08 (4)	–	7.14 ± 0.24 (10)	7.29 ± 0.15 (1)	–	7.40 ± 0.16 (2)	–	7.42 ± 0.04 (3)	7.01 ± 0.14 (10)
Cl	–	–	–	–	–	–	–	–	–	–
K	–	–	–	–	–	–	–	–	–	–
Ca	6.58 ± 0.26 (20)	6.70 ± 0.12 (17)	6.46 ± 0.09 (3)	5.66 ± 0.21 (22)	6.60 ± 0.14 (14)	6.20 ± 0.15 (6)	6.53 ± 0.20 (22)	5.60 ± 0.25 (5)	6.37 ± 0.12 (22)	6.11 ± 0.17 (49)
Sc	2.91 ± 0.06 (7)	3.33 ± 0.07 (11)	2.95 ± 0.11 (2)	2.59 ± 0.09 (9)	3.30 ± 0.14 (7)	2.69 ± 0.19 (4)	3.18 ± 0.10 (9)	2.70 ± 0.20 (5)	3.14 ± 0.09 (10)	2.93 ± 0.17 (21)
Ti	4.92 ± 0.15 (31)	5.03 ± 0.18 (36)	4.99 ± 0.19 (9)	4.93 ± 0.19 (67)	4.93 ± 0.12 (35)	4.61 ± 0.10 (7)	5.13 ± 0.13 (28)	4.58 ± 0.23 (11)	4.83 ± 0.13 (52)	4.73 ± 0.19 (180)
V	4.37 ± 0.17 (2)	4.50 ± 0.15 (7)	–	4.66 ± 0.17 (10)	4.18 ± 0.15 (2)	–	4.61 ± 0.16 (2)	–	4.32 ± 0.29 (8)	3.73 ± 0.19 (29)
Cr	5.60 ± 0.11 (29)	5.76 ± 0.14 (34)	5.47 ± 0.12 (3)	6.23 ± 0.15 (94)	5.58 ± 0.14 (25)	5.53 ± 0.15 (7)	5.66 ± 0.18 (25)	5.08 ± 0.15 (5)	5.50 ± 0.17 (55)	5.30 ± 0.20 (155)
Mn	5.32 ± 0.25 (6)	5.46 ± 0.16 (8)	5.30 ± 0.11 (1)	5.74 ± 0.19 (29)	5.28 ± 0.24 (9)	5.15 ± 0.16 (1)	5.08 ± 0.20 (8)	5.41 ± 0.18 (2)	5.05 ± 0.22 (16)	4.99 ± 0.26 (63)
Fe	7.47 ± 0.13 (95)	7.53 ± 0.08 (82)	7.44 ± 0.11 (17)	7.93 ± 0.13 (438)	7.39 ± 0.08 (62)	7.19 ± 0.13 (24)	7.47 ± 0.11 (87)	6.63 ± 0.18 (21)	7.27 ± 0.09 (154)	7.13 ± 0.12 (652)
Co	6.02 ± 0.17 (2)	5.59 ± 0.13 (2)	–	5.40 ± 0.05 (3)	6.36 ± 0.15 (1)	–	–	–	5.02 ± 0.17 (1)	4.62 ± 0.22 (27)
Ni	6.12 ± 0.19 (37)	6.49 ± 0.11 (27)	6.17 ± 0.11 (2)	6.96 ± 0.13 (100)	6.28 ± 0.13 (27)	5.85 ± 0.09 (3)	6.30 ± 0.15 (19)	5.50 ± 0.08 (7)	6.08 ± 0.16 (49)	5.86 ± 0.15 (157)
Cu	3.88 ± 0.37 (3)	4.17 ± 0.06 (3)	–	4.92 ± 0.16 (2)	4.42 ± 0.15 (2)	–	–	–	4.08 ± 0.17 (2)	3.73 ± 0.11 (5)
Zn	4.16 ± 0.17 (2)	4.83 ± 0.13 (2)	–	5.28 ± 0.04 (3)	4.53 ± 0.15 (2)	–	4.57 ± 0.16 (1)	3.70 ± 0.18 (1)	4.57 ± 0.17 (1)	4.18 ± 0.04 (4)
Ga	–	–	–	3.38 ± 0.16 (1)	–	–	–	–	2.96 ± 0.17 (1)	2.40 ± 0.22 (1)
Sr	3.41 ± 0.17 (1)	4.00 ± 0.13 (2)	–	4.00 ± 0.16 (2)	3.56 ± 0.15 (2)	0.79 ± 0.16 (1)	3.91 ± 0.16 (2)	0.61 ± 0.18 (1)	3.69 ± 0.17 (2)	2.66 ± 0.11 (3)
Y	1.97 ± 0.21 (4)	3.01 ± 0.19 (11)	–	3.04 ± 0.11 (17)	2.64 ± 0.10 (7)	–	2.62 ± 0.24 (4)	2.20 ± 0.18 (2)	2.53 ± 0.23 (16)	1.99 ± 0.25 (18)
Zr	3.31 ± 0.17 (2)	3.19 ± 0.20 (6)	–	3.00 ± 0.16 (3)	3.06 ± 0.22 (6)	–	3.64 ± 0.16 (2)	–	3.01 ± 0.11 (9)	2.45 ± 0.26 (24)
Ba	2.66 ± 0.10 (3)	3.60 ± 0.14 (3)	3.60 ± 0.11 (1)	3.80 ± 0.16 (5)	3.04 ± 0.15 (2)	1.88 ± 0.16 (2)	3.58 ± 0.19 (3)	1.32 ± 0.18 (1)	2.79 ± 0.21 (3)	2.31 ± 0.09 (5)
La	0.60 ± 0.17 (1)	1.60 ± 0.22 (3)	–	2.18 ± 0.16 (2)	1.32 ± 0.15 (1)	–	–	–	1.63 ± 0.22 (3)	0.96 ± 0.19 (13)
Ce	1.94 ± 0.17 (2)	2.40 ± 0.13 (1)	–	2.79 ± 0.03 (10)	–	–	–	–	2.22 ± 0.17 (2)	1.60 ± 0.20 (34)
Pr	0.65 ± 0.17 (1)	–	–	1.67 ± 0.16 (2)	–	–	–	–	–	0.46 ± 0.34 (7)
Nd	1.38 ± 0.17 (1)	2.10 ± 0.10 (6)	–	2.40 ± 0.10 (10)	1.84 ± 0.15 (2)	–	2.42 ± 0.16 (1)	–	2.04 ± 0.18 (4)	1.29 ± 0.23 (35)
Sm	–	–	–	2.01 ± 0.16 (1)	–	–	–	–	–	0.93 ± 0.22 (2)
Eu	–	–	–	–	–	–	–	–	–	2.08 ± 0.22 (2)
Gd	–	–	–	–	–	–	–	–	–	1.03 ± 0.17 (3)
Dy	–	–	–	–	–	–	–	–	–	0.58 ± 0.28 (4)
Er	–	–	–	–	–	–	–	–	–	1.43 ± 0.22 (2)

Table B1 – *continued*

	KIC 6443122	KIC 6670742	KIC 7119530	KIC 7122746	KIC 7668791	KIC 7748238	KIC 7767565	KIC 7773133	KIC 7779339	KIC 8211500
C	8.39 ± 0.23 (4)	8.58 ± 0.05 (3)	8.18 ± 0.15 (3)	8.43 ± 0.07 (3)	8.29 ± 0.20 (13)	8.45 ± 0.15 (6)	8.21 ± 0.23 (5)	8.78 ± 0.11 (8)	8.36 ± 0.25 (27)	8.51 ± 0.11 (4)
N	–	–	–	–	7.99 ± 0.16 (1)	–	–	–	8.17 ± 0.19 (1)	–
O	8.99 ± 0.16 (1)	9.11 ± 0.16 (2)	8.66 ± 0.22 (2)	8.86 ± 0.17 (2)	8.92 ± 0.16 (2)	8.78 ± 0.16 (1)	8.53 ± 0.17 (2)	8.94 ± 0.16 (1)	8.58 ± 0.19 (2)	8.82 ± 0.18 (2)
Ne	–	–	–	–	–	–	–	–	–	–
Na	7.04 ± 0.16 (2)	–	6.77 ± 0.22 (1)	5.85 ± 0.17 (1)	6.79 ± 0.10 (4)	6.65 ± 0.16 (2)	6.42 ± 0.17 (2)	6.51 ± 0.15 (4)	5.75 ± 0.12 (7)	6.46 ± 0.18 (2)
Mg	7.37 ± 0.08 (4)	7.86 ± 0.19 (5)	7.71 ± 0.17 (5)	7.76 ± 0.16 (7)	7.82 ± 0.07 (9)	7.87 ± 0.16 (5)	8.06 ± 0.24 (8)	7.70 ± 0.09 (9)	7.45 ± 0.18 (10)	7.95 ± 0.18 (5)
Al	–	–	–	–	6.77 ± 0.16 (1)	–	–	–	6.25 ± 0.19 (2)	–
Si	7.40 ± 0.24 (14)	7.34 ± 0.27 (3)	7.86 ± 0.29 (6)	7.31 ± 0.40 (7)	7.56 ± 0.19 (15)	7.74 ± 0.22 (10)	7.77 ± 0.21 (17)	7.62 ± 0.24 (22)	7.28 ± 0.21 (36)	7.36 ± 0.18 (7)
P	–	–	–	–	–	–	–	–	–	–
S	7.39 ± 0.11 (3)	–	–	6.92 ± 0.17 (1)	7.46 ± 0.26 (5)	7.59 ± 0.16 (2)	7.27 ± 0.17 (2)	7.47 ± 0.02 (3)	7.06 ± 0.13 (9)	7.63 ± 0.18 (2)
Cl	–	–	–	–	–	–	–	–	–	–
K	–	–	–	–	–	–	–	–	–	–
Ca	6.25 ± 0.25 (12)	6.17 ± 0.11 (7)	6.44 ± 0.12 (6)	6.32 ± 0.17 (12)	6.52 ± 0.16 (29)	6.65 ± 0.14 (13)	6.51 ± 0.20 (23)	6.62 ± 0.19 (24)	6.40 ± 0.18 (41)	6.18 ± 0.23 (13)
Sc	2.86 ± 0.12 (6)	3.32 ± 0.29 (4)	3.29 ± 0.30 (6)	3.26 ± 0.15 (5)	3.23 ± 0.17 (10)	3.18 ± 0.19 (6)	3.30 ± 0.09 (8)	3.40 ± 0.24 (11)	3.10 ± 0.19 (16)	2.99 ± 0.23 (5)
Ti	4.86 ± 0.12 (17)	4.86 ± 0.15 (8)	5.08 ± 0.10 (8)	5.13 ± 0.12 (18)	5.19 ± 0.13 (47)	5.01 ± 0.16 (20)	5.32 ± 0.21 (31)	5.32 ± 0.19 (55)	4.93 ± 0.18 (115)	5.13 ± 0.20 (20)
V	4.61 ± 0.16 (2)	–	–	–	4.41 ± 0.14 (5)	4.79 ± 0.16 (2)	4.96 ± 0.15 (4)	4.41 ± 0.27 (5)	4.02 ± 0.24 (18)	4.04 ± 0.18 (1)
Cr	5.65 ± 0.17 (16)	5.63 ± 0.14 (5)	5.68 ± 0.23 (5)	5.58 ± 0.14 (10)	5.79 ± 0.18 (59)	5.55 ± 0.16 (15)	6.00 ± 0.14 (31)	5.92 ± 0.16 (49)	5.41 ± 0.23 (125)	5.88 ± 0.14 (11)
Mn	5.21 ± 0.28 (7)	5.65 ± 0.16 (2)	5.71 ± 0.22 (2)	5.60 ± 0.17 (2)	5.29 ± 0.17 (11)	5.66 ± 0.20 (5)	5.23 ± 0.14 (8)	5.30 ± 0.25 (15)	5.01 ± 0.25 (35)	5.61 ± 0.14 (3)
Fe	7.50 ± 0.08 (45)	7.31 ± 0.11 (16)	7.38 ± 0.21 (19)	7.45 ± 0.12 (37)	7.46 ± 0.10 (117)	7.49 ± 0.11 (48)	7.75 ± 0.13 (98)	7.64 ± 0.11 (143)	7.13 ± 0.12 (352)	7.56 ± 0.09 (39)
Co	–	–	–	–	–	–	–	6.32 ± 0.16 (2)	4.81 ± 0.30 (16)	–
Ni	6.47 ± 0.22 (23)	5.93 ± 0.13 (3)	6.80 ± 0.31 (4)	6.21 ± 0.28 (9)	6.18 ± 0.19 (34)	6.43 ± 0.19 (18)	6.63 ± 0.14 (23)	6.22 ± 0.15 (47)	5.87 ± 0.17 (100)	6.51 ± 0.22 (11)
Cu	4.51 ± 0.16 (1)	–	–	–	4.19 ± 0.16 (2)	4.35 ± 0.16 (2)	4.43 ± 0.17 (1)	4.29 ± 0.16 (2)	3.35 ± 0.19 (1)	–
Zn	4.60 ± 0.16 (2)	–	–	4.39 ± 0.17 (1)	4.45 ± 0.16 (1)	–	4.76 ± 0.17 (2)	4.29 ± 0.16 (2)	3.97 ± 0.19 (2)	4.48 ± 0.18 (1)
Ga	–	–	–	–	–	–	–	–	–	–
Sr	3.43 ± 0.16 (1)	1.23 ± 0.16 (1)	1.48 ± 0.22 (1)	2.90 ± 0.17 (1)	3.93 ± 0.16 (1)	3.27 ± 0.16 (1)	4.10 ± 0.17 (2)	3.74 ± 0.16 (2)	3.20 ± 0.04 (3)	3.02 ± 0.18 (1)
Y	2.70 ± 0.09 (8)	–	2.68 ± 0.33 (3)	2.05 ± 0.17 (2)	2.55 ± 0.19 (10)	2.51 ± 0.24 (4)	2.95 ± 0.24 (6)	2.61 ± 0.20 (8)	2.30 ± 0.16 (19)	2.57 ± 0.28 (3)
Zr	2.90 ± 0.16 (2)	–	–	3.18 ± 0.17 (1)	2.78 ± 0.21 (10)	3.63 ± 0.04 (3)	3.14 ± 0.17 (4)	3.09 ± 0.20 (7)	2.92 ± 0.13 (19)	3.45 ± 0.18 (1)
Ba	3.13 ± 0.16 (2)	3.01 ± 0.16 (1)	2.64 ± 0.22 (2)	2.29 ± 0.17 (2)	2.53 ± 0.16 (2)	2.61 ± 0.16 (2)	3.85 ± 0.09 (4)	3.10 ± 0.16 (2)	2.89 ± 0.23 (4)	3.37 ± 0.18 (2)
La	1.52 ± 0.16 (1)	–	–	–	1.49 ± 0.16 (2)	–	2.45 ± 0.17 (2)	1.37 ± 0.16 (2)	1.29 ± 0.19 (11)	–
Ce	–	–	–	–	2.27 ± 0.22 (4)	–	2.63 ± 0.17 (1)	2.02 ± 0.16 (1)	1.69 ± 0.22 (34)	–
Pr	–	–	–	–	–	–	–	–	1.08 ± 0.19 (2)	–
Nd	–	–	–	–	2.38 ± 0.16 (2)	–	2.60 ± 0.17 (2)	1.65 ± 0.14 (3)	1.44 ± 0.26 (31)	–
Sm	–	–	–	–	–	–	–	–	1.43 ± 0.19 (2)	–
Eu	–	–	–	–	–	–	–	–	0.30 ± 0.19 (2)	–
Gd	–	–	–	–	–	–	–	–	1.19 ± 0.08 (3)	–
Dy	–	–	–	–	–	–	–	–	1.37 ± 0.04 (4)	–
Er	–	–	–	–	–	–	–	–	1.38 ± 0.19 (1)	–

Table B1 – *continued*

	KIC 8222685	KIC 8694723	KIC 8827821	KIC 8881697	KIC 9229318	KIC 9349245	KIC 9408694	KIC 9410862	KIC 9650390	KIC 9656348
C	8.07±0.11 (5)	8.19±0.06 (9)	8.15±0.10 (3)	8.72±0.25 (3)	8.60±0.24 (9)	8.38±0.16 (13)	8.59±0.19 (20)	8.33±0.22 (10)	8.61±0.15 (1)	8.31±0.26 (15)
N	–	–	–	–	–	8.40±0.15 (1)	–	–	–	–
O	8.92±0.14 (1)	–	8.66±0.15 (1)	9.14±0.19 (2)	9.12±0.16 (2)	8.78±0.07 (4)	9.08±0.24 (1)	–	8.95±0.15 (1)	8.68±0.23 (2)
Ne	–	–	–	–	–	–	–	–	–	–
Na	6.51±0.14 (1)	5.85±0.11 (7)	6.32±0.15 (2)	–	6.95±0.21 (4)	7.18±0.21 (6)	6.52±0.17 (9)	6.03±0.11 (9)	–	6.20±0.28 (3)
Mg	7.50±0.08 (5)	7.22±0.12 (11)	7.99±0.15 (7)	7.95±0.14 (6)	7.92±0.14 (8)	8.11±0.12 (9)	7.82±0.17 (13)	7.54±0.05 (8)	8.07±0.15 (2)	7.51±0.19 (6)
Al	–	–	–	–	6.67±0.16 (1)	–	5.78±0.17 (1)	5.78±0.17 (1)	–	–
Si	7.47±0.25 (11)	7.24±0.28 (34)	7.64±0.23 (12)	7.53±0.25 (5)	7.73±0.18 (16)	7.93±0.20 (23)	7.67±0.29 (44)	7.32±0.19 (46)	7.29±0.19 (3)	7.03±0.25 (10)
P	–	–	–	–	–	–	–	–	–	–
S	7.14±0.14 (2)	7.00±0.17 (2)	7.55±0.15 (2)	7.83±0.19 (1)	7.57±0.11 (3)	7.50±0.11 (7)	7.47±0.16 (11)	7.06±0.17 (2)	–	6.58±0.23 (1)
Cl	–	–	–	–	–	–	–	–	–	–
K	–	–	–	–	–	–	–	–	–	–
Ca	6.27±0.13 (12)	5.99±0.16 (47)	6.59±0.20 (15)	6.50±0.20 (7)	6.67±0.18 (17)	6.87±0.18 (22)	6.58±0.19 (38)	6.22±0.18 (33)	6.56±0.14 (4)	5.85±0.12 (16)
Sc	2.85±0.08 (5)	2.85±0.10 (23)	3.43±0.13 (6)	3.16±0.20 (5)	3.55±0.04 (6)	3.38±0.13 (7)	3.62±0.13 (13)	2.88±0.10 (16)	3.77±0.24 (5)	2.38±0.25 (5)
Ti	4.77±0.09 (19)	4.65±0.16 (111)	5.11±0.12 (16)	5.07±0.23 (15)	5.42±0.13 (25)	5.30±0.17 (33)	5.25±0.20 (89)	4.74±0.15 (117)	4.88±0.09 (5)	4.40±0.20 (34)
V	4.61±0.14 (1)	3.28±0.26 (11)	4.92±0.15 (2)	4.07±0.19 (1)	4.85±0.25 (5)	4.81±0.15 (5)	4.63±0.23 (13)	3.57±0.15 (22)	–	4.07±0.22 (5)
Cr	5.52±0.14 (13)	5.18±0.17 (105)	5.69±0.22 (15)	5.78±0.18 (8)	5.96±0.17 (25)	5.97±0.14 (33)	5.79±0.22 (97)	5.30±0.17 (110)	5.98±0.13 (5)	5.01±0.20 (27)
Mn	5.14±0.15 (4)	4.94±0.19 (32)	5.43±0.15 (3)	5.67±0.19 (2)	5.75±0.26 (6)	5.74±0.10 (6)	5.25±0.24 (29)	4.97±0.19 (32)	6.13±0.15 (1)	4.65±0.34 (7)
Fe	7.20±0.07 (47)	7.02±0.10 (431)	7.60±0.07 (34)	7.49±0.11 (26)	7.75±0.08 (53)	7.92±0.11 (89)	7.53±0.13 (338)	7.19±0.13 (427)	7.59±0.11 (13)	6.84±0.11 (81)
Co	–	4.60±0.12 (7)	–	–	5.41±0.16 (1)	6.40±0.15 (2)	5.04±0.22 (11)	4.70±0.06 (15)	–	4.73±0.23 (2)
Ni	6.05±0.18 (15)	5.76±0.12 (91)	6.47±0.17 (14)	6.42±0.19 (6)	6.61±0.14 (31)	6.89±0.16 (45)	6.28±0.15 (87)	5.93±0.15 (138)	6.66±0.15 (2)	5.86±0.37 (27)
Cu	4.23±0.14 (2)	3.66±0.10 (3)	4.80±0.15 (2)	–	5.24±0.16 (2)	4.62±0.15 (2)	4.10±0.11 (4)	3.78±0.01 (3)	–	4.13±0.23 (2)
Zn	4.47±0.14 (2)	4.24±0.17 (2)	4.40±0.15 (1)	4.66±0.19 (1)	4.46±0.16 (1)	5.18±0.15 (2)	4.61±0.24 (2)	4.18±0.08 (3)	–	3.98±0.23 (2)
Ga	–	2.48±0.17 (1)	–	–	–	–	3.91±0.24 (2)	–	–	–
Sr	3.01±0.14 (1)	2.72±0.17 (2)	3.66±0.15 (1)	3.00±0.19 (1)	4.00±0.16 (1)	3.40±0.15 (1)	3.63±0.25 (3)	3.24±0.17 (1)	2.42±0.15 (1)	2.96±0.23 (2)
Y	2.22±0.31 (3)	1.75±0.14 (14)	2.63±0.21 (3)	1.63±0.19 (1)	2.89±0.21 (7)	2.70±0.18 (7)	2.42±0.14 (11)	1.65±0.15 (16)	1.90±0.15 (1)	1.71±0.23 (7)
Zr	2.73±0.14 (2)	2.49±0.28 (19)	3.04±0.14 (3)	3.12±0.19 (1)	3.22±0.08 (4)	3.13±0.33 (4)	2.95±0.20 (14)	2.75±0.34 (6)	–	2.58±0.08 (5)
Ba	2.17±0.14 (2)	2.22±0.15 (4)	3.14±0.15 (2)	2.76±0.19 (2)	3.08±0.16 (2)	3.62±0.14 (5)	2.76±0.16 (5)	2.13±0.25 (4)	–	1.65±0.35 (3)
La	0.77±0.14 (1)	0.89±0.24 (4)	1.74±0.15 (1)	–	2.16±0.16 (2)	2.57±0.11 (3)	1.48±0.14 (8)	0.96±0.27 (5)	–	1.16±0.23 (2)
Ce	–	1.44±0.14 (16)	–	–	2.25±0.16 (2)	2.59±0.10 (4)	1.85±0.21 (15)	1.44±0.14 (10)	–	1.47±0.26 (3)
Pr	–	0.20±0.17 (2)	–	–	–	–	1.26±0.33 (3)	0.72±0.17 (1)	–	–
Nd	–	1.12±0.20 (12)	–	–	2.21±0.16 (1)	2.45±0.15 (2)	1.72±0.26 (14)	1.11±0.26 (18)	–	1.75±0.23 (2)
Sm	–	0.70±0.17 (1)	–	–	–	–	1.25±0.24 (1)	2.10±0.17 (1)	–	–
Eu	–	0.68±0.17 (1)	–	–	–	–	–	–	–	–
Gd	–	1.11±0.17 (1)	–	–	–	–	1.77±0.24 (2)	–	–	–
Dy	–	0.80±0.17 (1)	–	–	–	–	1.67±0.24 (2)	–	–	–
Er	–	–	–	–	–	–	–	–	–	–

Table B1 – *continued*

	KIC 9828226	KIC 9845907	KIC 9941662	KIC 9970568
C	8.43 ± 0.16 (2)	7.90 ± 0.20 (19)	8.25 ± 0.34 (4)	7.86 ± 0.24 (2)
N	–	7.58 ± 0.18 (1)	–	–
O	8.89 ± 0.16 (1)	8.57 ± 0.04 (3)	8.55 ± 0.20 (1)	9.26 ± 0.24 (1)
Ne	–	–	–	–
Na	–	6.08 ± 0.15 (7)	6.66 ± 0.20 (1)	6.66 ± 0.24 (1)
Mg	6.52 ± 0.16 (2)	7.47 ± 0.13 (13)	7.73 ± 0.22 (4)	7.74 ± 0.27 (5)
Al	–	6.15 ± 0.18 (1)	–	–
Si	6.60 ± 0.16 (2)	7.34 ± 0.16 (24)	7.73 ± 0.14 (6)	6.89 ± 0.34 (4)
P	–	–	–	–
S	–	7.02 ± 0.20 (8)	7.54 ± 0.20 (1)	7.94 ± 0.24 (2)
Cl	–	–	–	–
K	–	–	–	–
Ca	6.21 ± 0.16 (2)	6.01 ± 0.11 (32)	5.69 ± 0.19 (8)	6.37 ± 0.21 (8)
Sc	3.24 ± 0.16 (2)	2.61 ± 0.12 (9)	2.94 ± 0.54 (3)	3.14 ± 0.25 (3)
Ti	3.91 ± 0.13 (4)	4.79 ± 0.15 (78)	5.13 ± 0.16 (16)	5.18 ± 0.25 (12)
V	–	4.27 ± 0.21 (20)	4.70 ± 0.20 (2)	–
Cr	4.71 ± 0.16 (4)	5.39 ± 0.20 (84)	6.07 ± 0.19 (10)	5.41 ± 0.30 (8)
Mn	–	5.23 ± 0.20 (32)	5.20 ± 0.13 (4)	4.91 ± 0.24 (2)
Fe	6.37 ± 0.21 (11)	7.10 ± 0.11 (272)	7.63 ± 0.06 (39)	7.34 ± 0.09 (21)
Co	–	5.18 ± 0.04 (3)	–	–
Ni	–	5.79 ± 0.23 (62)	6.49 ± 0.11 (8)	6.07 ± 0.28 (6)
Cu	–	3.93 ± 0.18 (2)	–	–
Zn	–	–	4.54 ± 0.20 (1)	4.90 ± 0.24 (1)
Ga	–	–	–	–
Sr	–	2.61 ± 0.18 (2)	3.89 ± 0.20 (1)	1.99 ± 0.24 (1)
Y	–	2.11 ± 0.19 (8)	2.94 ± 0.20 (2)	3.14 ± 0.24 (2)
Zr	–	2.57 ± 0.19 (16)	2.95 ± 0.20 (1)	2.93 ± 0.24 (1)
Ba	1.23 ± 0.16 (1)	2.01 ± 0.14 (4)	3.97 ± 0.20 (2)	3.47 ± 0.24 (2)
La	–	1.43 ± 0.13 (3)	–	–
Ce	–	2.05 ± 0.17 (9)	–	–
Pr	–	–	–	–
Nd	–	1.44 ± 0.28 (6)	–	–
Sm	–	–	–	–
Eu	–	0.87 ± 0.18 (2)	–	–
Gd	–	–	–	–
Dy	–	–	–	–
Er	–	1.65 ± 0.18 (1)	–	–

This paper has been typeset from a TEX/LATEX file prepared by the author.